frontiers in Neuroscience

TYPE Methods
PUBLISHED 04 November 2026
DOI 10.3389/fnins.2026.1983186

Check for updates

OPEN ACCESS

EDITED BY
Claire-Marie Rangon,
Hôpital Raymond-Poincaré, France

REVIEWED BY
Marco Carner,
Integrated University Hospital Verona, Italy
Jisung Kim,
Seoul National University Hospital, Republic of Korea

*CORRESPONDENCE
Matthew P. Ward
mpward@purdue.edu

RECEIVED 30 August 2026
REVISED 07 October 2026
ACCEPTED 15 October 2026
PUBLISHED 04 November 2026

CITATION
Wilson D, Shader MJ, Steinhubl SR and Ward MP (2026) TEMPO-taVNS: a multimodal platform optimizing thermal, electrical, and mechanical auricular stimulation.
Front. Neurosci. 20:1983186.
doi: 10.3389/fnins.2026.1983186

COPYRIGHT
© 2026 Wilson, Shader, Steinhubl and Ward. This is an open-access article distributed under the terms of the Creative Commons Attribution License (CC BY). The use, distribution or reproduction in other forums is permitted, provided the original author(s) and the copyright owner(s) are credited and that the original publication in this journal is cited, in accordance with accepted academic practice. No use, distribution or reproduction is permitted which does not comply with these terms.

TEMPO-taVNS: a multimodal platform optimizing thermal, electrical, and mechanical auricular stimulation

Damen Wilson[1,2], Maureen J. Shader[3], Steven R. Steinhubl[1] and Matthew P. Ward[1,2]*

[1]Weldon School of Biomedical Engineering, Purdue University, West Lafayette, IN, United States, [2]School of Medicine, Indiana University, Indianapolis, IN, United States, [3]Speech, Language, and Hearing Sciences, Purdue University, West Lafayette, IN, United States

Transcutaneous auricular vagus nerve stimulation (taVNS) is typically delivered electrically, while alternative stimulation modalities and their potential for personalization remain underexplored. We present TEMPO-taVNS (Thermal, Electrical, and Mechanical Parameter Optimization for taVNS), a human-centered methodology for multimodal auricular neuromodulation designed to explore and optimize stimulation of sensory pathways associated with the auricular branch of the vagus nerve (ABVN). The platform integrates custom hardware capable of delivering thermal, vibrotactile, and electrical stimulation with software that enables systematic parameter sweeps. Responses are characterized through high-resolution physiological monitoring including heart rate, heart rate variability, gastric slow-wave activity, pupil diameter, beat-to-beat blood pressure, brain response activity, and electrodermal activity, together with participant-reported perception and comfort. To address interindividual variability, a Pareto-front Gaussian-process optimization framework identifies personalized stimulation parameters by balancing physiological response with user comfort. We further describe experimental protocols for evaluating this multimodal parameter space in humans. Together, the hardware, software, physiological sensing, and optimization framework provide a scalable foundation for individualized, non-invasive and non-pharmacological auricular neuromodulation, and for investigating non-electrical approaches to vagal stimulation for wearable neuromodulation systems.

KEYWORDS
auricular branch of vagus, multimodal stimulation, taVNS, thermal stimulation, vagus nerve stimulation, vibrotactile

1 Introduction

Transcutaneous auricular vagus nerve stimulation (taVNS) is an emerging biomodulation therapeutic strategy targeting the afferent sensory branch of the vagus nerve located on the ear, known as the auricular branch of the vagus nerve (ABVN) (Kaniusas et al., 2019b). taVNS is intended to recruit sensory afferents of the auricular branch of the vagus nerve (ABVN). taVNS has been shown to activate the nucleus tractus solitarius (NTS), the main vagal afferent target, which in turn projects to the locus coeruleus (LC), a region also shown to be activated with taVNS (Sclocco et al., 2019; Butt et al., 2020). Translational research has accordingly split into two main branches: one examining traditional vagus autonomic modulation, the other

examining LC noradrenergic (LC-NA) effects on the central nervous system (Kaniusas et al., 2019a). Applications range from heart failure and POTS to depression and insomnia. Due to the noninvasive, non-pharmacological nature of electrical taVNS, it is considered very safe with adverse effects reported in prior studies limited to skin irritation, headache, and nasopharyngitis (Redgrave et al., 2018; Tyler et al., 2019; Kim et al., 2022).

The ABVN innervates the cymba concha on the ear, with several areas of overlap with the auriculotemporal nerve and greater auricular nerve in other parts like the tragus, helix, antihelix, and concha (Butt et al., 2020). The ABVN originates from the jugular ganglion on each side and forms peripheral branches and communicates with the facial and, variably, glossopharyngeal nerves. Because the jugular ganglia exchange communicating fibers with the glossopharyngeal and facial nerves, the exact afferent pathways of the ABVN remain ambiguous (Butt et al., 2020). When stimulating the ABVN via taVNS applied to the cymba concha, fMRI has shown that primary area of activation in the brainstem is the NTS, the same place where vagal trunk afferents project to Butt et al. (2020). Furthermore, when observing retrograde nerve tracing in animals, the evidence highlights that the ABVN and cervical vagal trunk both supply the NTS widely, but the greater auricular nerve and auriculotemporal nerve (CN V) primarily activate the trigeminal nucleus and tract, cuneate nucleus, and cervical nuclei instead of majority NTS (Butt et al., 2020; Das and Breiner, 2026). With this evidence in mind, despite inconsistent taVNS results to date, it stands to reason that reflexes projecting through the NTS could be potentially elicited or mimicked utilizing the ABVN. Two autonomic reflexes related to this path are the trigeminocardiac reflex and diving reflex. The trigeminocardiac reflex is defined as gastric hypermotility, hypotension, and bradycardia following thermal or mechanical stimulation of the trigeminal nerve (Lemaitre and Schaller, 2015). The diving reflex is thought to be a subtype of the trigeminocardiac reflex, and often associates with hypertension instead of hypo, and is elicited by the holding of breath while submerging the face in cold water (Lemaitre and Schaller, 2015). These reflexes transform somatosensory information through the sensory nucleus of V and then project efferents through to the nucleus ambiguous and dorsal motor nucleus (Panneton and Gan, 2020; Gutierrez et al., 2023). These latter two nuclei are two main projection targets from the NTS, especially in vagal modulation. A variation of these somatosensory pathways or reflexes may be present in our neural circuity, able to be manipulated with taVNS, as evidenced with gastric, cardiac, and blood pressure modulation observed with some applications of taVNS (Antonino et al., 2017; Kaniusas et al., 2019a; Steidel et al., 2021; Zhu et al., 2021).

Several groups hypothesize C-fibers are responsible for the therapeutic efficacy in cervical vagus nerve stimulation, while others credit Aβ fibers (Woodbury and Woodbury, 1990; Krahl et al., 2001). Meanwhile, in the auricular vagus, most if not all published work has investigated Aβ fiber activation due to limits on device current magnitude with perceived pain. This is further perturbed by the fact that less than a fifth of the ABVN is comprised of Aβ fibers (Safi et al., 2016). Thus, if conventional tolerable electrical taVNS predominantly recruits Aβ fibers, only a subset of the total ABVN fiber population may be accessible under these stimulation conditions. Differences in personal pain tolerance may account for why some individuals exhibit physiological responses to taVNS while others do not. Principally, when discussing cervical VNS, efficacy is primarily determined by seizure reduction not autonomic symptoms or type of fiber engagement (Krahl et al., 2001). However, distinct vagal afferent subpopulations could mediate separate functional outcomes; for example, ascending projections of a specific region or fiber caliber type may project to thalamocortical networks to drive seizure suppression, whereas other fiber types may lead to connections to brainstem autonomic nuclei to trigger efferent cardiovascular and respiratory reflexes. In fact, inflammatory cytokine mediation, an autonomic effect of the vagus, has been shown to be tied to specific C and Aδ cervical murine vagus fibers (Zanos et al., 2018). To investigate the autonomic effect, if any, of C or Aδ fiber recruitment in a human auricular vagus nerve, there needs to be non-painful excitation methodology created and tested. Without a limit on pain thresholds, there may be much greater physiological effects of taVNS that have yet to be explored.

To date, taVNS has primarily used electrical stimulation and has shown inconsistent effects on autonomic activity as measured by expected changes in heart rate. For example, a meta-analysis of 15 studies involving 563 people receiving taVNS showed that nearly half showed no change in cardiac activity (Verma et al., 2021). Therefore, there is much room for improvement in optimizing and innovating upon taVNS to elicit consistent and predictable effects. To our knowledge, there are no studies observing non-electrical taVNS in the form of thermal. However, a few studies have investigated non-electrical taVNS in the form of vibrotactile on autonomic outcomes in humans. Addorisio et al. (2019) applied mechanical oscillatory vibrations to the cymba concha of healthy controls for two minutes with timed blood draws subjected to endotoxin stimulation. Compared to sham, they found vibrotactile taVNS significantly reduced TNF-α, IL-1, and IL-6, demonstrating an efficacious reduction of inflammatory response (Addorisio et al., 2019). Another cohort within the study investigated the effect on Rheumatoid Arthritis (RA) patients, and showed reduction of Visual Analog Scale scores and DAS28 scores (an RA disease score) (Addorisio et al., 2019). Interestingly, after these brief taVNS treatments, inflammatory markers remained reduced up to 24 h in healthy patients, and in RA patients the scores remained reduced for 7 days (Addorisio et al., 2019). While cardiac effects were not measured, the anti-inflammatory effects elicited via non-electrical stimulation seem promising for the technique's viability. Cognitive modulation is the other target effect for prior vibrotactile taVNS work. Tan et al. (2024) found that when vibrotactile stimuli delivered to the cymba concha, the stimulation was able to improve working memory in their N-back task paradigm (Tan et al., 2024). Furthermore, Donovan et al. (2025) found that vibrotactile taVNS was able to alter limbic brain regions and their coherence (Donovan et al., 2025). Of note, prior studies tested a limited range of frequencies on their vibration, Addorisio et al. at ~168 Hz, Tan et al. at 6 Hz, and Donovan et. at 2, 6, 12, 20, and 40 Hz (Addorisio et al., 2019; Tan et al., 2024; Donovan et al., 2025). Consequently, systematic exploration across a continuous and wider frequency band is required to determine optimal engagement of auricular mechanoreceptive pathways and overcome the limitations of single or sparse frequency protocols.

Current protocols for electrical taVNS applications often utilize a calibration method of increasing stimulus current at a fixed pulse width and frequency until just before a participant feels pain or discomfort (Sclocco et al., 2019, 2020). Given advances in biometric technology and sensing, it serves to reason that there is enormous potential to improve the calibration methodology such as utilization in advanced continuous health monitoring and the rise in affordable wearable technology. Frei and Osorio (2001) found that in cervical vagus nerve stimulation, effects on HR were highly variable as a group,

but yet very consistent on an individual level (Frei and Osorio, 2001). Given this as well as the inconsistent physiological effects of taVNS, it is logical to postulate that taVNS parameters and methodologies need to be personalized for each individual such that their unique settings elicit predictable and durable physiologic changes necessary for symptom remediation. Furthermore, in its current state, taVNS is open loop, and interest in growing in creating closed-loop applications for it (Yu et al., 2021; Dabiri et al., 2022). Efforts have primarily focused on using closed-loop taVNS by focusing on the timing of application as the feedback method as opposed to individual physiological parameters but still seen promising results (Yu et al., 2021; Dabiri et al., 2022).

To our knowledge, this work represents the first integrated hardware and experimental platform designed to perform systematic parameter sweeps of electrical, vibrotactile and thermal auricular stimulation, including controlled heating and cooling. The platform combines stimulation delivery with synchronized acquisition of a broad range of physiological and behavioral signals, including pupillometry, beat-to-beat blood pressure, cardiac activity, electrodermal activity, electrogastrography, electroencephalography, functional near infrared spectroscopy (fNIRS), and perceptual responses. These multimodal measurements are incorporated into a personalized, multi-objective Pareto optimization framework to identify stimulation parameters that balance physiological efficacy and participant tolerability. Here, we describe the design, verification, and implementation of the TEMPO-taVNS (Thermal, Electrical, and Mechanical Parameter Optimization for taVNS) platform and demonstrate its use as a framework for developing highly individualized auricular neuromodulation protocols.

2 Materials and methods

All procedures described within this manuscript were done under IRB protocol #2025-00000076, approved by the Purdue Institutional Review Board on Feb. 12, 2026.

2.1 Recording equipment

An overview of the experimental equipment is described below, with minor deviation depending on which session the participant was in at the time. Participants are tethered to a lead I electrocardiogram (ECG), a 3-lead cutaneous electrogastrogram (EGG), virtual reality (VR) headset, galvanic skin response (GSR) recording electrodes, either two-channel EEG (Cz and Pz) or eight optode fNIRS (dependent on session), in ear headphones, and the stimulator apparatus (dependent on session). All equipment including the bed platform and headphones are sanitized between each use with healthcare hydrogen peroxide based cleaner.

2.1.1 Cutaneous electrodes

For each electrode, the skin is first cleaned with an alcohol prep pad to ensure optimal contact. The Ag/AgCl electrodes (Red Dot 2239, 3 M Health Care, St. Paul, MN, USA) then are attached using adhesive collars and secured with a small amount of conductive gel (axion Contact Gel, axion GmbH, Leonberg, Germany). ECG electrodes are placed in a standard lead I configuration to measure the electrocardiogram. To measure the electrogastrogram, electrodes are placed with the positive lead on left midclavicular line, two inches below the xiphoid process and negative lead halfway between naval and xiphoid process. Both ECG and EGG were first passed into an ADInstruments FE238 Octal Bio Amp and then an ADInstruments PowerLab. The Galvanic Skin Response (GSR) is recorded with electrodes placed on the palmar surface of the distal phalanges (finger pads) of the index and middle fingers of the participant's right hand. It first is passed through an ADInstruments GSR Amp FE116, then to the ADInstruments PowerLab DAQ. These three signals are recorded via LabChart recording software on a dedicated PC. GSR, ECG, and EGG are recorded at a sampling rate of 10 kHz timestamped in Unix time.

2.1.2 Non-invasive blood pressure

Beat-to-beat noninvasive blood pressure (NIBP) is recorded using an INL382 Human NIBP Nano System (ADInstruments). The wrist cuff is secured around the participant's right wrist, and the finger cuff is placed on the middle finger.

2.1.3 Virtual reality

The Varjo XR-4 VR headset is used for two purposes: to continuously measure pupil diameter and to display subjective perception and comfort-related surveys to users while in a supine position. The pupil diameter is sampled at 200 Hz in Varjo software, with time stamps in Unix to align with LabChart data post hoc. The surveys (described in section 2.3.6) are displayed in the Augmented Reality (AR) space.

2.1.4 Electroencephalography

EEG is recorded using a two-channel montage at Cz and Pz to provide redundant measurements of auditory evoked responses. For each channel, the non-inverting (active) electrode is positioned at the corresponding scalp location according to the international 10–20 system, with the inverting (reference) electrode placed at the contralateral mastoid. The ground electrode is tied to a common ground from the Lead I ECG setup. The leads are plugged into the ADInstruments FE238 Octal Bio Amp, which in turn feeds a data stream to the ADInstruments PowerLab DAQ. EEG data was recorded at 10 kHz sample rate in the LabChart software with Unix timestamps.

2.1.5 Functional near infrared spectroscopy

In sessions 4–5, fNIRS data is recorded using the NIRx NIRScout recording system. Data is recorded from eight optodes (C6, T8, CP4, CP6, TP8, P4, P6, P8), positioned according to the international 10–20 system to target right temporal and parietal cortical regions. Source detector separation is maintained at ~3 cm. Signals are continuously recorded at 100 Hz with Unix time, with dual wavelength illumination to allow estimation of changes in oxyhemoglobin and deoxyhemoglobin concentrations. Optode placement is secured with a cap designed for stable contact and minimal light leakage.

2.1.6 Audio

To allow flexibility for research involving the cognitive space, such as tinnitus applications, we included audio integration paradigm in

the methodology. Each user undergoes an audiogram prior to beginning session 1 utilizing Apple AirPods Pro 3 and an iPad, implementing Apple's built in Hearing Test software. Etymotic ER3SE headphones are used for auditory stimuli during the experiment, with 3 different sized disposable memory foam tips to help ensure a proper fit for each user. The ER3SE headphones are plugged into the M-Audio M-Track Solo USB Audio Interface, set to 62 dB SPL output. Two sound stimuli are used, described in section 2.3.7 and were created in Audacity software and played through LabChart software according to triggers.

2.2 Stimulating equipment

2.2.1 Vibrotactile stimulator

For vibrotactile taVNS, the Precision Microdrives Model No. 308-107 8 mm mini vibration motor is used. It was applied in a custom-made earpiece (Figure 1). The earpiece was custom designed in Fusion 360 and 3D-printed via fused deposition modeling (P1S, Bambu Lab, Shenzhen, China; 0.4 mm nozzle) using polylactic acid filament (1.75 mm PLA, SUNLU, Zhuhai, China) at a layer height of 0.2 mm. The device is controlled by an Arduino, which drives a MOSFET (NTR4101PT1G) to variable power from a 3.6 V/1A power supply. The vibrotactile stimulator was operated using two drive regimes. For stimulation frequencies ≥60 Hz, the motor was driven continuously at the voltage corresponding to the desired operating frequency. Because stable continuous rotation at 10 and 20 Hz was below the practical operating range of the motor, these two conditions were instead generated using software-controlled pulsed operation. For the 10- and 20-Hz conditions, the motor was supplied at 1.76 V and switched on and off using software-timed delay loops at repetition rates of 10 and 20 Hz, respectively. Thus, these conditions represent 10- and 20-Hz pulse repetition rates rather than continuous motor rotation at those frequencies.

2.2.1.1 Vibrotactile hardware verification

The continuously driven operating range of the vibrotactile stimulator was quantitatively characterized prior to experimental use. Vibratory output was measured using an Adafruit ADXL335 triple-axis analog accelerometer rigidly mounted to the vibrating surface of the stimulator. The accelerometer output was acquired using an ADInstruments PowerLab DAQ at a sampling frequency of 10 kHz. Across the continuously driven voltage settings, acceleration data were recorded over 10 repeated trials of 5 s duration. The dominant vibration frequency was determined using spectral analysis (FFT), and peak and RMS acceleration were calculated. These measurements were used to characterize the relationship between applied voltage, vibration frequency, acceleration, and trial-to-trial variability shown in Figure 2. The software-gated 10- and 20-Hz conditions described above were not included in this bench characterization.

2.2.2 Thermal stimulator

The same custom hardware and configuration (Figure 3) is used for thermal heating and cooling. A custom Peltier-based thermal stimulator with configurable, graded outputs is used to determine the subjective perception and perceived comfort of different levels of hot and cold stimulation. It is adapted from Sperduti et al.'s design of a thermal stimulator (Sperduti et al., 2025). We utilized the same 15 × 15 mm Peltier cell (Adaptive, United Kingdom). For the custom tip, we designed a similar tip except, here we use a 6 mm diameter tip, machined in copper (Figure 3). We utilize a custom water loop dissipating into a standardized generic 120 mm CPU cooler radiator on the heatsink side of the Peltier. The tip with Peltier is affixed into a custom mounting apparatus. This custom apparatus helps to lower and raise the thermode for controlling contact with the skin surface (Z positioning) and provides precise +/− 1 mm position control to facilitate repeatable consistency in transducer placement (Figure 3). To ensure safety and regulatory compliance, the Peltier cell is powered

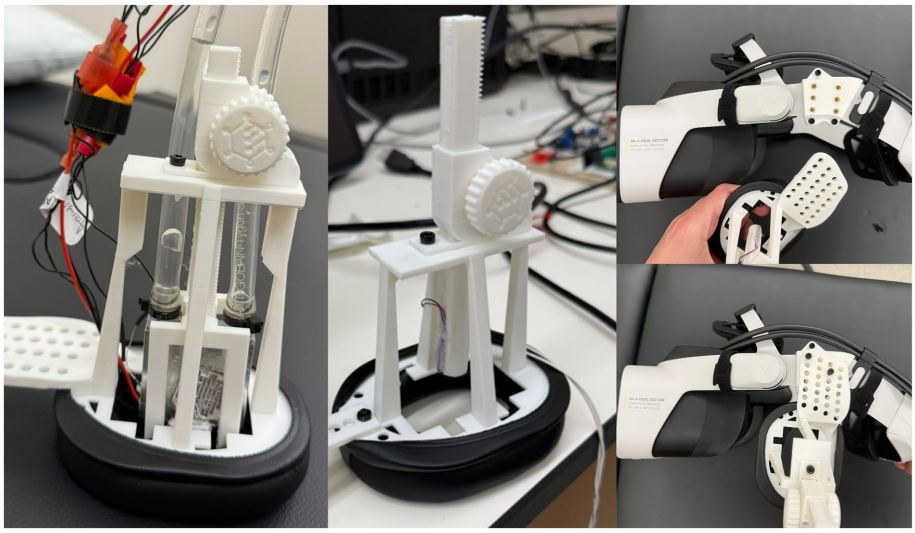

FIGURE 1
Custom thermal and vibrotactile auricular taVNS stimulators and VR headset mounting system. (Left) Thermal stimulator assembly housed within a custom-designed, 3D-printed support structure. (Center) Vibrotactile stimulator enclosed within its custom-designed, 3D-printed housing. (Right) Upper and lower views demonstrating the custom attachment mechanism used to mount the stimulator assemblies to the Varjo virtual reality headset, shown disengaged from the mounting interface (top) and secured in the mounted position (bottom).

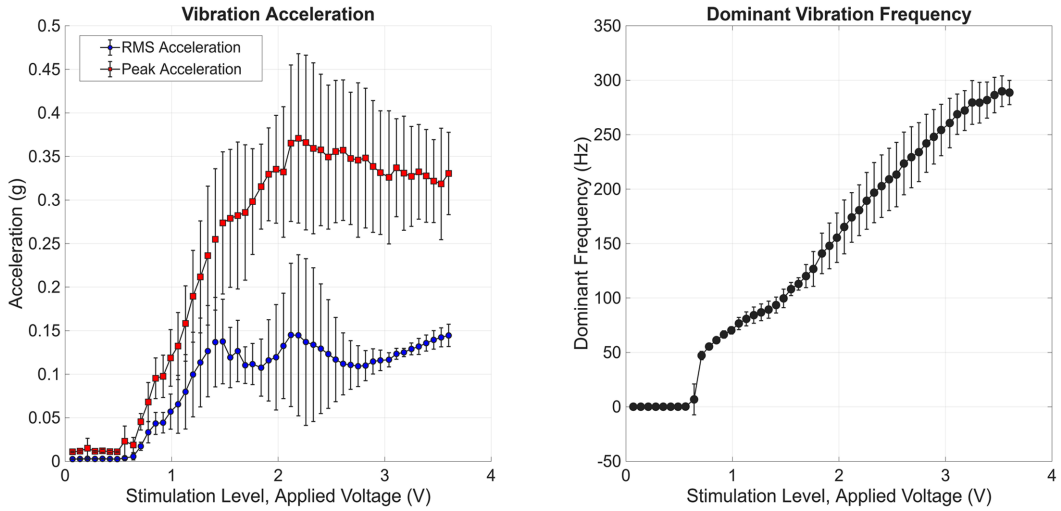

FIGURE 2
Left figure shows the root-mean-square (RMS) acceleration (blue circles) and peak acceleration (red squares) of the vibrotactile stimulator as a function of the applied input voltage (analogous to stimulation level). Right figure shows the dominant vibration frequency across all stimulation settings, demonstrating an operational onset threshold near 0.7 V followed by a near-linear frequency increase up to ~290 Hz at maximum voltage. Error bars represent ± SD across 10 repeated measurements (n = 10).

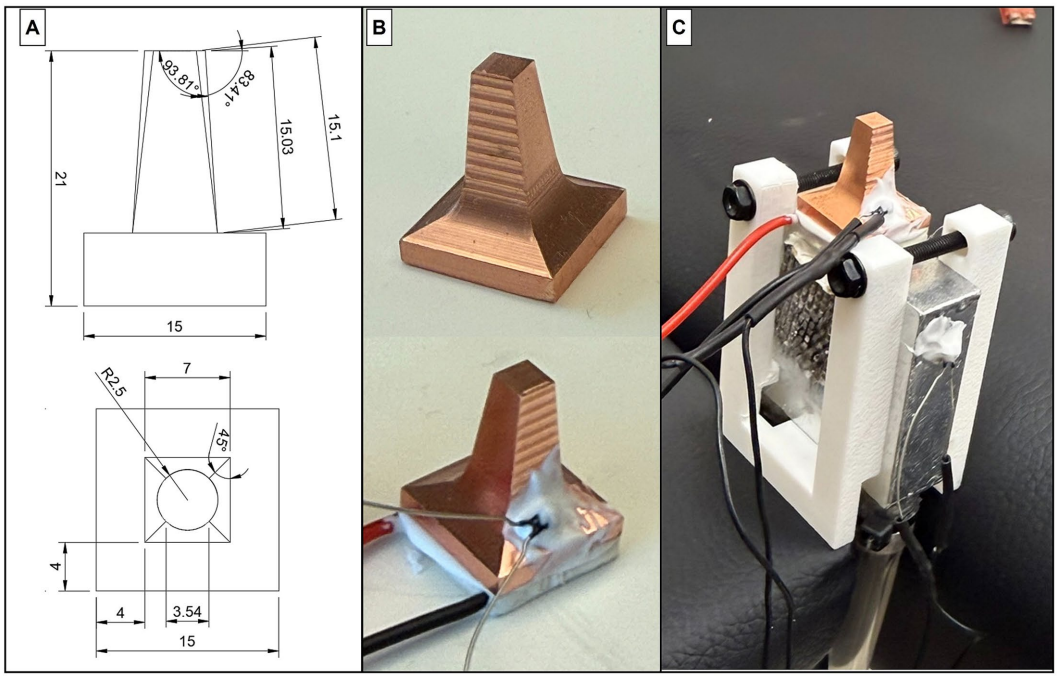

FIGURE 3
Custom-designed copper thermode assembly. **(A)** Computer-aided design (CAD) schematic of the machined copper thermal tip with dimensions indicated in millimeters (mm). **(B)** Photograph of the machined copper thermode featuring a precision thermistor secured with thermal epoxy and a Peltier thermoelectric cooler (TEC) fixated to the base. **(C)** Fully assembled unit including the water-cooling block and integrated mounting hardware for experimental fixation.

by a rigorously certified medical-grade supply (CUS60M-12, 12 V, 60 W; TDK-Lambda), meeting IEC/EN/ES 60601-1 3rd and 4th edition standards with robust 2 × MOPP isolation and BF-rated compliance. This powers the thermoelectric controller (TEC-1091; Meerstetter Engineering), which provides high precision and reliability. We implement software enforced current and temperature limits to prevent unsafe operation, with an upper bound of 60 °C and/or 4 A, and a lower bound of 0 °C. An overview of the custom hardware for control of the thermode as well as vibrotactile stimulator is shown in Figure 4.

Since the thermode is applied in 4 out of the 5 sessions, to mitigate variability between uses, we maintain a custom-made mold out of Play-Doh (Hasbro, Inc., Pawtucket, RI), a non-toxic modeling compound, with a metal cylinder placed inside, used to mark the thermode position on the cymba concha. During the first session the thermode is used, we take the new malleable and formable Play-Doh

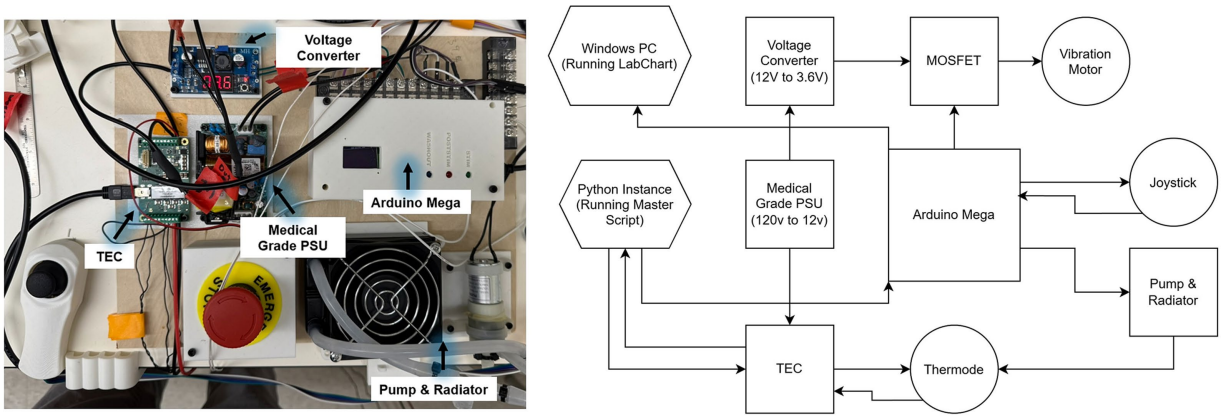

FIGURE 4
Custom control and power distribution unit for thermal and vibrotactile stimulation apparatus. A high-amperage power chain and control architecture drive the thermode system. Internal view of the custom-machined housing containing an Arduino Mega microcontroller and integrated wiring terminal blocks. Power regulation stage illustrating the transition from 120 V AC line voltage via a medical-grade power supply and step-down converter to 3.6 V DC high-amperage output. Thermal management system featuring a TEC-1091 controller for Peltier voltage regulation, coupled with a liquid-cooling pump and radiator assembly for heat dissipation.

and place an aluminum cylinder in it. Next, we mark the cylinder with a colored marker, then press the compound into the auricle cymba concha region of the ear. A two mm circle is left upon removal of the compound, serving as the target for our thermode. After the first session, the mold is allowed to harden and be safely stored and labeled for subsequent sessions. A similar procedure is followed in subsequent test sessions (Supplementary Figure 1). The primary investigator maintains a manual override emergency stop button and will terminate the procedure if the participant shows visible signs of distress or if the device appears to be malfunctioning. Furthermore, the thermoelectric controller is set to a limit of heating at 60 °C and limit of cooling at 0 °C, per safety standards often used in quantitative sensory testing (Sperduti et al., 2025).

2.2.2.1 Thermal hardware verification

Thermode performance was quantified using time to target, average hold temperature, mean absolute error during the hold period, overshoot, and trial-to-trial precision. Time to target was defined as the time from the commanded temperature change to the first measured sample within the target range. Average hold temperature was calculated over the 30 s target hold period. Mean absolute error was calculated as the average absolute difference between the measured and target temperatures during the hold. Overshoot was defined as the maximum deviation beyond the target temperature following a transition. Precision was quantified across repeated trials using the coefficient of variation (CV). CV was determined as (SD/mean × 100%) using temperatures expressed in °C. Because CV calculated from Celsius temperatures is dependent on the temperature scale, the corresponding between-trial SD in °C is also reported as a scale-appropriate measure of absolute temperature variability.

Heating and cooling rate bench characterization was performed using the maximum achievable transition rate of the thermode rather than the controlled 0.5 °C/s ramp rate that will be used in future participant testing. This characterization was intended to establish the dynamic operating limits of the thermal system across the tested temperature range. During participant testing, the controller instead commanded a target ramp rate of 0.5 °C/s. This rate was maintained across the majority of the experimental temperature range; however, at lower target temperatures (approximately <17 °C), the maximum cooling capability of the system could fall below 0.5 °C/s, resulting in a correspondingly slower transition to the target temperature. Thus, the variable rates reported in Figure 5 represent the maximum achievable thermal transition rates and not the programmed ramp rates used in the participant protocol.

2.2.3 Electrical stimulator

Electrical taVNS is applied with bipolar constant current stimulation from an isolated stimulator (ADInstruments Stimulator HC FE155) to the cutaneous receptive field formed by the auricular branch of the vagus nerve in the outer ear via the cymba concha (Peuker and Filler, 2002). Conductive rubber carbon electrodes formed into an ear clip serve as the stimulating electrodes (Supplementary Figure 2). The skin is first cleaned with an alcohol prep pad to ensure optimal contact, and a small amount of conductive gel is placed on electrode pads before placement on the cymba concha. The stimulus is 10 Hz, 0.8 ms, with current amplitude (mA) being determined by each user's subjective verbal rating of 4 out of 10 (0: no sensation, 10: distressing pain) (Ward et al., 2020). During the calibration, the stimulus current (mA) is increased from 0.1 mA in 0.1 mA increments until the participant verbally scores the 4 out of 10. Stimulation administration is controlled via ADInstruments PowerLab DAQ and LabChart software.

2.3 Stimulation protocol

Overall, the TEMPO-taVNS protocol is designed as five separate sessions per participant, as shown in Supplementary Figure 3 and described in Supplementary Table 1. The first three sessions comprise parameter exploration (vibrotactile, heating, and cooling), followed by two personalized multimodal evaluation sessions. In the present methods study, Session 1 (vibrotactile stimulation) was completed in a single participant to demonstrate implementation of the integrated stimulation, synchronized multimodal recording, subjective assessment, analysis, and

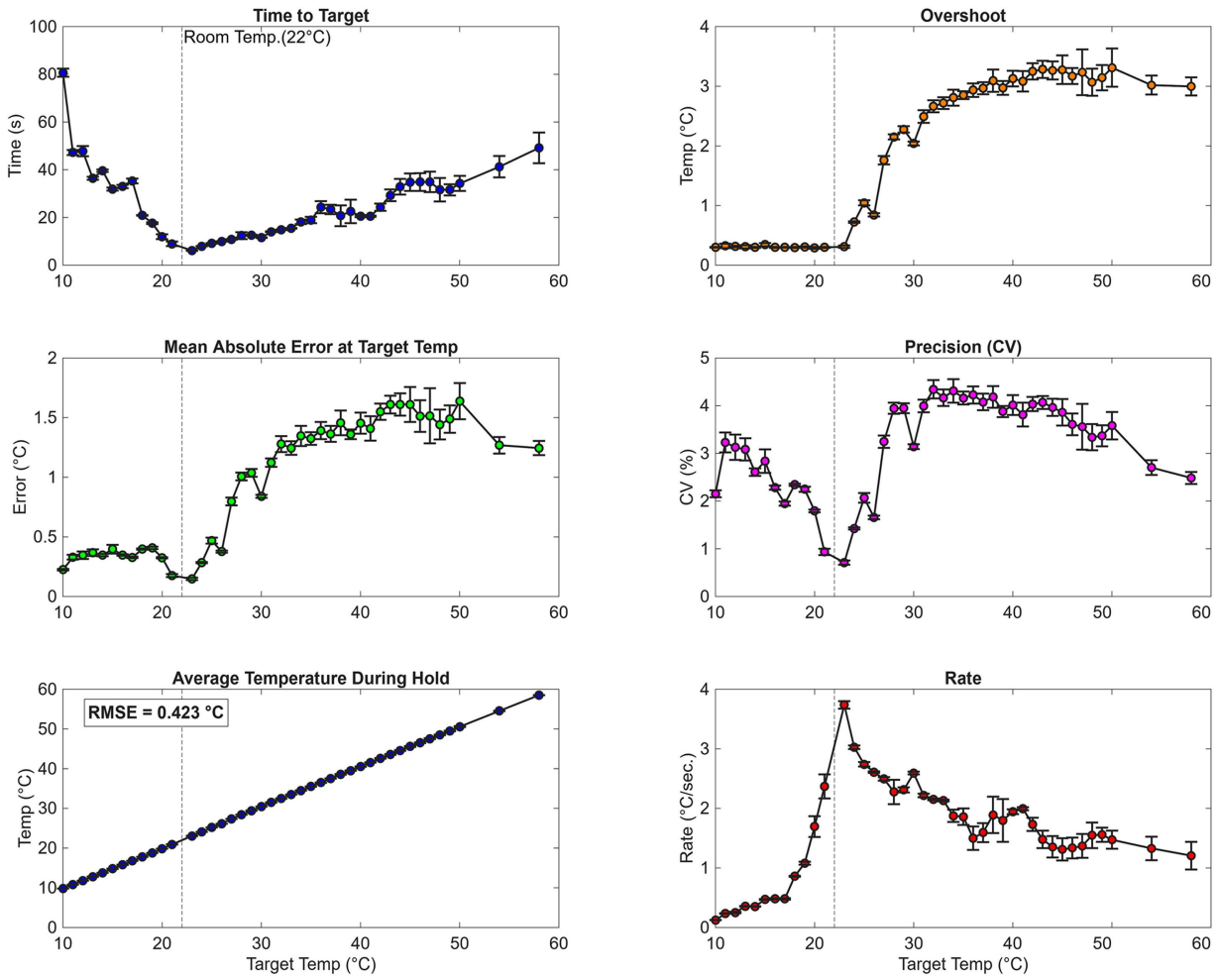

FIGURE 5
Performance characterization of the TEC-based thermode across target temperatures. Thermal performance was evaluated across a range of programmed target temperatures, with room temperature indicated by the vertical dashed line at 22 °C. Each panel shows one performance metric as a function of target temperature. Time to target was shortest near room temperature and increased for target temperatures farther from ambient, particularly for cooling targets below room temperature. Overshoot and mean absolute error were lowest near and below room temperature and increased at higher target temperatures. Trial-to-trial precision, quantified as the coefficient of variation (CV), remained within a low percentage range across the tested temperatures, with increased variability at select temperatures. Average temperature during the hold period closely tracked the programmed target temperature across the full tested range, with an overall RMSE of 0.423 °C. Heating and cooling rate varied with target temperature, with the fastest rates observed near the transition above room temperature and lower rates at more extreme targets. Points indicate mean values across trials (n = 10), and error bars indicate standard deviation across repeated measurements.

parameter-optimization workflow. Sessions 2–5 are presented as the planned extension of this framework and were not evaluated in participants in the present report. Accordingly, the participant results reported here are intended to demonstrate methodological feasibility rather than the efficacy of vibrotactile, thermal, or electrical taVNS.

2.3.1 Session 1 (vibrotactile taVNS)

Figure 6 provides an overview of the vibrotactile taVNS evaluation protocol. Participants first undergo a baseline measurement period of 5 min. The parameter exploration block is 9 levels of vibration tested at 5 repeats each on the cymba concha: 0 Hz (control), 10 Hz, 20 Hz, 60 Hz, 100 Hz, 133 Hz, 167 Hz, 200 Hz, and 220 Hz. The 0-Hz control condition follows the same epoch structure as the active vibrotactile conditions, including auditory stimulation, continuous comfort reporting, subsequent perception and sensation surveys, VR presentation, and positioning of the stimulation apparatus, but without activation of the vibrotactile motor. The selection of these test frequencies was informed by the types of mechanoreceptors present in the skin of the cymba concha. In the non-glabrous skin of the ear, there are rapidly adapting hair follicle receptors, found to maximally respond to 20 Hz (Lechner and Lewin, 2013). Additionally, there are Pacinian Corpuscles mechanoreceptors that optimally respond to 200 Hz (Sato, 1961; Bolanowski and Verrillo, 1982; Onishi et al., 2021). Furthermore, it is thought that Merkel cells, or touch domes, as well as some Pacini Corpuscles may contribute to frequency perception around 100 Hz (Schmidt et al., 2023). Due to the wide variability in human vibration perception experiments and variation in mechanoreceptor sensitivity themselves, we chose additional levels to test at around these three frequencies (Strzalkowski et al., 2017; Kawai and Tanaka, 2022; Verrillo, 1966). We selected points above the highest of 200 Hz and below the lowest of 20 Hz, and then equally spaced levels between, resulting in the 9 levels. The survey prompts present in each epoch are described in the

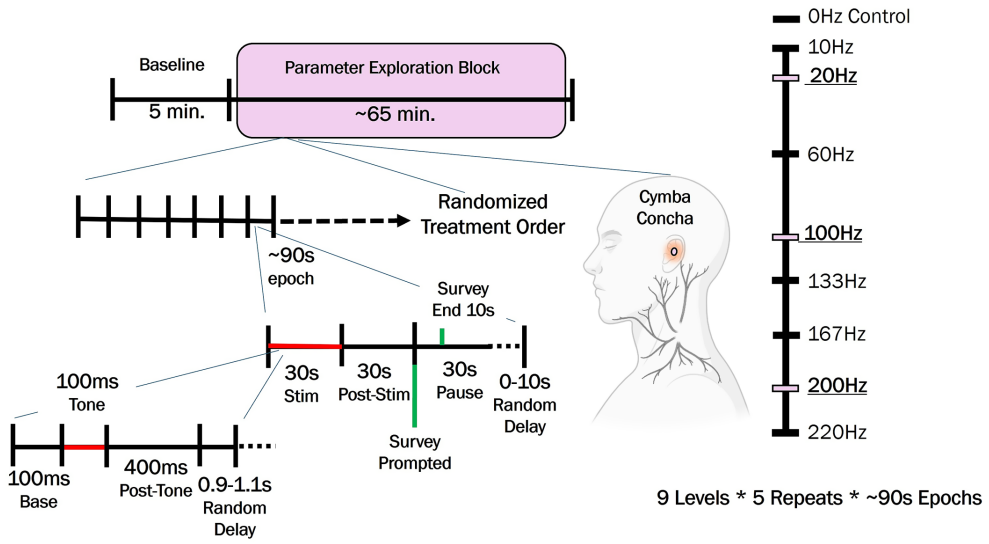

FIGURE 6
Vibrotactile taVNS session overview with two distinct baseline and parameter exploration blocks. During the parameter exploration block, stimuli are randomly presented in 90 s epochs. Auditory stimuli are applied throughout each stimulation epoch. The settings at which vibration parameters are set are shown on the right-hand side. Source: BioRender. License: BioRender Academic Publication Licenses, Agreement No. GB2ACMBQ15. Created in BioRender. Wilson, D. (2026) https://BioRender.com/yewiz1v.

Surveys section 2.3.6 of the methods. Similarly, the auditory stimuli in the epoch are described in the *Auditory Stimuli* section 2.3.7.

2.3.2 Session 2 (thermal taVNS: heating)

In the second session, the parameters of heating are evaluated (Figure 7). Each participant first undergoes a sensory threshold test. In the Thermal Warm Sensation Threshold (TWST) test, we measure the warm detection threshold in which the participant first perceives a temperature warmer than skin temperature. We follow a protocol for this established prior by Lithfous et al. (2022) for cold sensory and pain thresholds, in which we use for session three (cooling) and inverted for session two to use for warm in this session (Lithfous et al., 2022). To start, the stimulator is set to a baseline temperature of 1 °C below the participant's local skin temperature, so that participants begin the task feeling neutral/cold rather than warm. The probe is then placed on the preauricular area of the left side of face and held on the skin for 5 s before stimulation begins. Warming stimulation is delivered at a speed of 0.5 °C/s for 500 ms per trial, followed by a 5 s pause to allow for responses, per prior work (Lithfous et al., 2022). The rate of warming was chosen as used in prior work due to human reaction time and minimum detectable temperature variation (Sperduti et al., 2025). Participants are instructed to press a button with their right hand as soon as they feel a warm sensation; if they do not respond within five seconds, the increment in trials proceeds with a step increase in temperature. An adaptive staircase method is used to determine thresholds as Lithfous et al. (2022) had previously done; step size decreases by half (beginning at 2 °C) at each response reversal (reversing between felt/not-felt) until reaching the minimum increment of 0.1 °C, which is then maintained. The final threshold is calculated as the mean of the final 10 reversals at the minimum 0.1 °C step size. For the Thermal Hot Pain Threshold (THPT) test, a protocol established by Sperduti et al. is used where the probe is placed on the preauricular area and heated at a rate of 0.5 °C/s, and the participant is asked to press the button in their right hand at the first feeling of discomfort due to the stimulus (Sperduti et al., 2025). Upon the button press, the probe is immediately retracted from participants' skin and cooled. This process is repeated nine times to get an average of their THPT (Sperduti et al., 2025). Regardless of detection or pain, the probe has a limit of heating to 60 °C (Sperduti et al., 2025).

After thermal sensitivity thresholds are determined, there is a 5-minute period of baseline physiology recordings while the participant is lying in a supine position with no movement or talking. Next, the parameter exploration block begins, where 9 levels of heating are tested with 5 repeats each in 90 s epochs. The 9 heating levels relative to baseline local skin temperature are determined as such: Δ0 °C (control), Δ2 °C below TWST, TWST °C, five Equi spaced levels between TWST °C and Δ2 °C below THPT, and Δ2 °C below THPT. The 2 °C safety margin below the participant-specific hot pain threshold (THPT) is applied to the realized thermal trajectory rather than solely to the nominal target setpoint. The software incorporates the characterized heating overshoot when defining allowable stimulation temperatures such that a commanded target is not permitted if the target temperature plus the expected overshoot would encroach within 2 °C of the participant's measured THPT. Thus, the highest allowable heating setpoint could be reduced below the nominal THPT −2 °C condition when necessary to accommodate the transient overshoot of the thermode.

As shown in Figure 7, the pre-stimulation, stimulation, and post-stimulation recording windows comprised 90 s of fixed-duration recording; however, the total trial duration was longer and variable because it additionally included the thermal ramp, randomized timing intervals, and subsequent survey completion. In particular, the stimulus descriptor survey had no fixed completion time. The stimulation consists of the thermal probe on the cymba concha heated at a rate of 0.5 °C/s to assigned temperature level. Once the target temperature is reached, the 30-s stimulation period begins, during which the thermode maintains the assigned

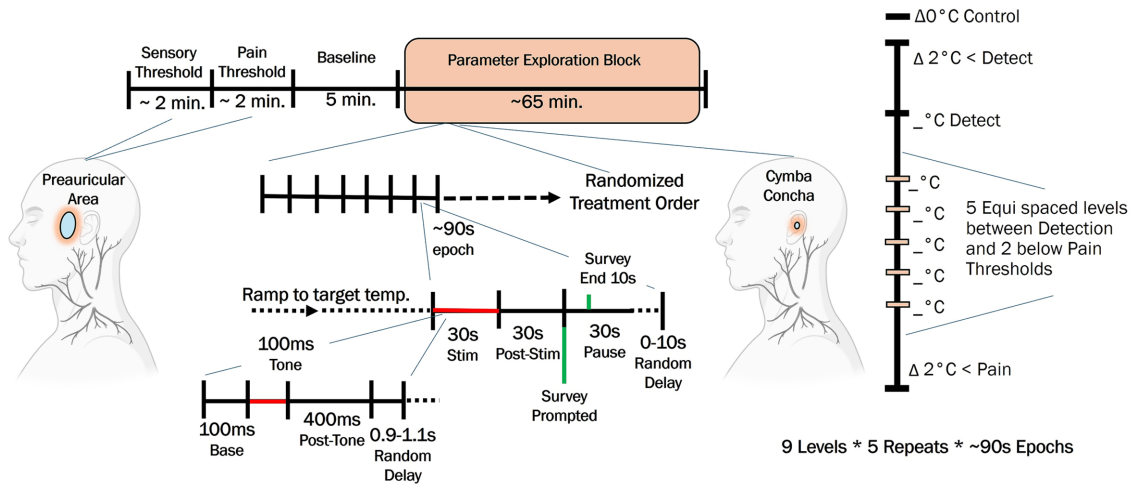

FIGURE 7
Thermal taVNS session overview with four distinct periods of sensory thresholding, pain thresholding, baseline, and parameter exploration. During the parameter exploration block, stimuli are randomly presented in 90 s epochs. Auditory stimuli are applied throughout each stimulation epoch. The settings at which temperature parameters are set are shown on the right-hand side, where levels are determined in reference to thresholds unique to each individual. Source: BioRender. License: BioRender Academic Publication Licenses, Agreement No. GB2ACMBQ15. Created in BioRender. Wilson, D. (2026) https://BioRender.com/yewiz1v.

target temperature, after which it returns to baseline skin temperature. A 30-second stimulus duration was selected for two reasons. First, electrical taVNS and VNS studies looking at acute effects of stimulation have found HR modulation occurring and stabilizing with 30–40 s of administration, often even much earlier (Badran et al., 2018; Austelle et al., 2024). Second, cutaneous thermal sensation in humans requires up to 3 s and 7 s for cooling and heating respectively to stabilize skin tissue and maximally activate thermoreceptors. Thirty seconds should therefore provide ample time for activation (Luo et al., 2020). Similarly to activation periods, the 30 s post-stimulation and ~30 s pause should provide ample recovery time to prevent rollover into the next trial, as prior work has shown cardiac recovery from acute stimulation is rapid (Badran et al., 2018; Austelle et al., 2024). The order of treatment levels is completely randomized for each participant using Python's *random.shuffle()* function, ensuring every possible sequence of treatments is equally likely.

2.3.3 Session 3 (thermal taVNS: cooling)

The experimental protocol for cooling stimulation follows the identical procedures described for heating stimulation except for minor adjustments to testing cooling as opposed to warming. The baseline probe temperature is set 1 °C above the measured skin temperature to ensure participants initially perceive neutral/warm rather than a cold sensation (Lithfous et al., 2022). The same adaptive staircase procedure, randomization of stimulus order using a Python script, and probe placement are applied as with session two thermal taVNS testing. For both the Thermal Cool Sensation Threshold (TCST) and Thermal Cold Pain Threshold (TCPT), participants press a button upon perceiving a cooling sensation or pain rather than a warming one. Furthermore, a lower temperature limit of 0 °C is to be enforced (Sperduti et al., 2025).

The parameter exploration period is identical to session two aside from the treatment level selection. It is analogous to the heating session, but relative to the TCPT and TCST consisting of 9 levels: Δ0°C (control), Δ2°C above TCST, TCST °C, 5 Equi spaced levels between TCST °C and Δ2°C above TCPT, and Δ2°C above TCPT. All other methodological details remain unchanged from the heating session.

2.3.4 Parameter optimization selection

We utilize an analysis pipeline between sessions three and four to identify candidate optimal stimulus parameter settings for each participant. For this proof-of-concept study, "optimal" was operationally defined as the safe and tolerable setting that most closely approximated the prespecified multivariate response profile presented in Supplementary Table 2. This profile favored decreases in HR, SBP, and SCL and increases in RMSSD, EGG amplitude, N1-P2 amplitude, pupil diameter, and subjective comfort. The combined decrease in HR and increase in RMSSD was interpreted as a pattern consistent with greater cardiac parasympathetic modulation. Lower SCL and greater comfort discouraged the selection of settings associated with nonspecific sympathetic arousal or poor tolerability, whereas the other outcomes provided complementary cardiovascular (SBP), gastrointestinal (EGG), and central-response (N1-P2 amplitude, pupil diameter) information. Thus, the selected setting represents a protocol-specific compromise across outcomes rather than a universally optimal taVNS parameter set.

To identify the candidate optimal stimulus parameters across multiple physiological and subjective outcomes, we implement a multi-objective optimization framework using Gaussian Process Regression (GPR) and Pareto analysis (Deb et al., 2002; Choinière et al., 2024). We use the five repeat measurements at each parameter for the following eight metrics: HR, RMSSD, SBP, EGG, SCL, N1P2 amplitude, pupil diameter, and subjective comfort. For each outcome, the five repeated observations at each parameter level are first averaged to obtain a single response value per tested frequency. Gaussian process regression is then fit to the resulting parameter-level means

using MATLAB *fitrgp* with a squared-exponential kernel, constant basis function, standardized predictor and response, exact fitting and prediction, and a fixed noise standard deviation of 0.40 in standardized-response units. GPR posterior means are evaluated within the experimentally tested range (example, 0–220 Hz), without extrapolation. Multi-objective optimization is performed using *gamultiobj* with a population size of 250, a maximum of 250 generations, a Pareto fraction of 0.70, and a fixed random seed of 1. All objectives are equally weighted, and no uncertainty penalty is applied. Pareto solutions are normalized across objectives. To select a single optimal candidate set of stimulation parameters from the Pareto set, we use a distance-to-ideal approach: each Pareto solution is normalized, and its Euclidean distance to the ideal point is computed, defined as the combination of best achievable values across all metrics. This goal of best achievable values is shown in Supplementary Table 2. The solution with the smallest distance is designated the most optimal candidate set of stimulation parameters. This approach enables systematic, data driven identification of stimulation parameters that balance multiple physiological and subjective outcomes. Candidate optimal vibrotactile, heating and cooling parameters are computed for each individual prior to further evaluation in sessions four and five. The analytical methods used ensure that the predicted optimal parameters will fall within the bounds of the participant's previously tolerated levels and will remain subject to the absolute safety cut-offs defined in sessions one and two.

2.3.5 Sessions 4 and 5 (all stimulus modalities)

Following completion of sessions one through three, participants come in for a higher repeat, more-tailored approach. The fourth and fifth sessions are identical; it is just necessary to split into two separate sessions due to the length of testing required. In these final two sessions, participants follow the session overview shown in Figure 8. Participants undergo four different blocks in randomized order. Each block consists of predetermined parameter levels, and all consist of an initial device fit period where the corresponding apparatus for the modality (e.g., thermal probe for thermal stimulation) is attached and fit to the participant's ear. Next, there is a two-minute pause for baseline adjustment prior to beginning the stimulation epochs. The stimulation epochs are identical to the previous sessions, except the fourth and fifth sessions use different auditory cues (see section 2.3.7). In these two final sessions, fNIRS is used instead of EEG for measuring auditory cortex activity; a higher repeat count of 15 is used to account for the use of fNIRS as opposed to five in previous sessions.

Parameters for vibrotactile and thermal taVNS are selected between the third and fourth session. For vibrotactile, heating, and cooling taVNS, each participant is stimulated with two parameters each. One parameter set for each of these modalities will be a standardized one, identical in level to everyone. The other parameter setting is a personalized one, tuned for each individual based on responses in sessions one through three. The standardized parameter for vibrotactile taVNS is 200 Hz, selected due to Pacinian corpuscles being tuned to this, likely the most prominent mechanoreceptor found in the outer ear (Sato, 1961; Bolanowski and Verrillo, 1982; Onishi et al., 2021). The standardized parameter for heating taVNS of +Δ3 °C was selected as prior work has shown that areas of the face and preauricular area in humans have a TWST of +Δ3 °C (Essick et al., 2004; Kim et al., 2013). The standardized parameter for cooling of −Δ5 °C was selected as prior work has shown that the TCST is often estimated to be around this −Δ5 °C (Lithfous et al., 2022; Sperduti et al., 2025). As for the electrical taVNS parameter, this is completed at 10 Hz, 0.8 ms pulse width, and a calibrated amplitude current. The 10 Hz was selected as it has been shown to induce autonomic cardiac effects in short trains as used in this study (Badran et al., 2018). The calibration procedure to determine current amplitude (mA) follows commonly used taVNS methodology from Sclocco et al. (2020) with a numeric

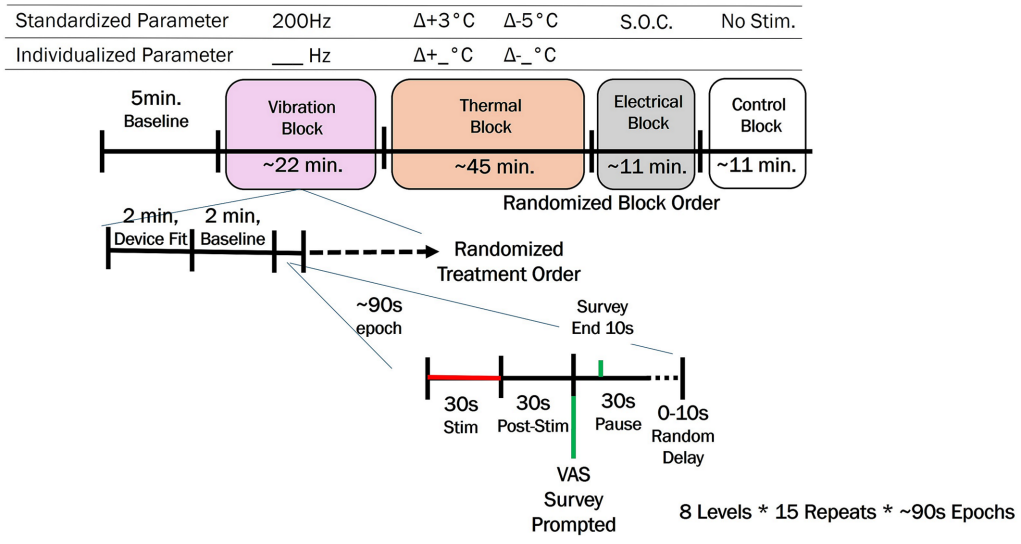

FIGURE 8
Tailored multimodal TEMPO-taVNS session overview with five distinct periods: baseline, vibration, thermal, electrical, and control. During each of the modality blocks (vibration, thermal, and electrical) the first few minutes are spent fitting each stimulus transducer type to the skin surface of the cymba concha. Next, a small baseline period ensues to mitigate stress or interreference from the transition of fitting. Then, the epochs begin, where stimulation is applied for 30 s with 30 s of post stimulation response recordings. Subjective sensation and comfort surveys are completed by the participant after this post stimulation period before moving to the next epoch. Auditory stimuli are applied throughout each stimulation epoch for proper fNIRS auditory stimuli recording.

rating scale (NRS) (Sclocco et al., 2019, 2020). For calibration, the stimulus current increases from 0.1 mA in 0.1 mA increments by the conductor until the participant verbally scores the level of sensation/discomfort as 4 out of 10 (0: no sensation, 10: distressing pain). Current intensity is set to achieve moderate to strong (but not painful) sensation (target score: 4/10), and this current intensity is the selected amplitude for the *standard of care* or "S.O.C" setting in the electrical block. The control block consists of the electrical taVNS hardware placed on the ear, but no stimulus is administered through them, only auditory stimuli are administered during the control block.

2.3.6 Parametric subjective sensation and comfort assessments

There are three types of surveys presented to participants throughout experiments during the interval between stimulation epochs. The surveys are displayed in virtual reality through the VR headset the participant will be wearing. Participants respond to surveys in VR while in a supine position using a joystick controller. Participants remain supine throughout data collection and view the same VR environment and survey interface across active and control conditions. Joystick interaction is limited to the standardized survey procedures described below. The slider bar surveys that gauge relative comfort/discomfort are completed by the participant with simple left and right movement of the joystick. For the subjective sensation survey, the joystick is used to highlight sensory descriptors and the button on the joystick (depression of joystick triggers button press) is used to toggle any boxes and finalize the entry. As part of the equipment setup, each participant is shown an instructional video regarding the experiment and surveys used. They are given time to read them ahead of time, ask for any clarification, and practice answering them with the controller. Once the experiment begins, there is to be no further instruction and survey questions are prompted just as shown in Figure 9.

The first survey presented to users is the comfort survey (Supplementary Figure 4) with descriptors at tick marks of: very uncomfortable, uncomfortable, just uncomfortable, just comfortable, comfortable, and very comfortable. This comfort survey is to gauge participant comfort with these new modalities of stimulation. This comfort assessment method was adapted from Ivanova et al. (2021) to gauge temperature comfort, with the gap between the two sides utilized to urge active answering as opposed to remaining neutral (Ivanova et al., 2021). Uniquely though, this survey is displayed during the entire stimulation period, with participants instructed that they could answer continuously during the 30 s period. This allows insight into potential temporal trends with comfort in previously unexplored stimulation modalities and how subjective assessment might change as a function of the length of stimulation. Furthermore, the slider is a continuous slider in that its position is not locked to the visible ticks. This was intentional as Lee et al. (2010) found with sensation testing that using this format as compared to full visual analog scale and complete categorical scale (ticks as the only answer inputs) was both more valid and sensitive in reporting (Lee et al., 2010).

The second survey displayed to users is upon completion of the post stimulation period (60 s after start of epoch, 30 s stimulation, 30 s post stimulation). This is a survey aimed at assessing one's sensation as a function of stimulus modality (thermal or vibrotactile) and applied stimulation parameters. For the thermal sessions of heating and cooling, users are prompted with, "How do you perceive the temperature?" For this, the tick labels used are: cold, cool, slightly cool, neutral, slightly warm, warm, and hot (Supplementary Figure 5).

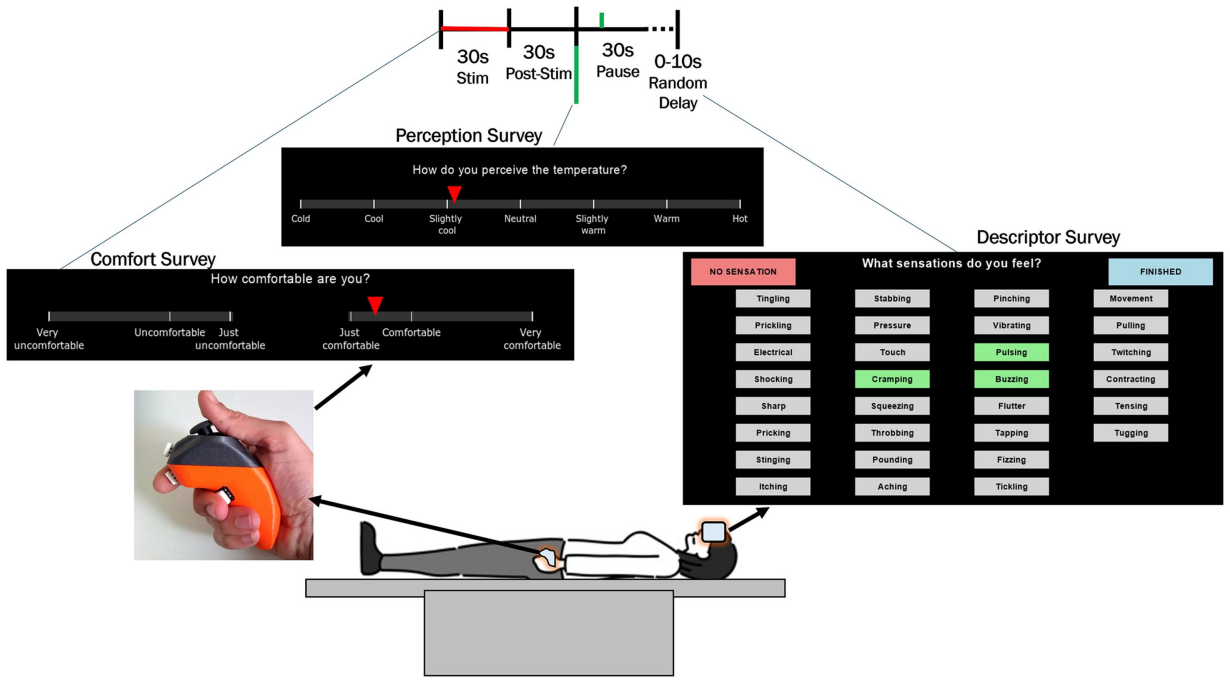

FIGURE 9
Overview of VR survey presentation to participant and mode of data entry. The participant sees all surveys projected into Augmented Reality space with the Varjo X4-4 headset. During the stimulation period, the participant can continuously answer/change their comfort rating. After the post stimulation recording period, they are prompted with a perception survey for 10 s, after which a descriptor survey appears. Stimulus descriptors survey modified from (Graczyk et al., 2022), thermal perception survey modified from (Ivanova et al., 2021; ISO 7730:2005, n.d.), and comfort survey modified from (Ivanova et al., 2021).

These descriptors were based on the ASHRAE thermal sensation survey (ISO 7730:2005, n.d.). To assess vibrotactile perception, we designed a 7-point Likert scale as used in other non-vibrotactile sensation studies (Lee et al., 2010; Joshi et al., 2015). The question we ask during these vibrotactile sessions is, "How do you perceive the strength of vibration?", noting that prior to experimentation both the highest and lowest are applied to the participant in the instructional tutorial to gather a frame of reference to go off; no other indictors or clues on reference are given after the blocks begin. The tick labels for descriptors on this scale are: very weak, weak, slightly weak, neither strong nor weak, slightly strong, strong, very strong. Furthermore, similar to the comfort survey, answers are administered with a joystick and the slider is a continuous slider in that its position is not locked to the visible ticks (Lee et al., 2010). Participants have 10 s to answer this survey, after the 10 s have passed, the survey records last position as response and moves to the next survey described below.

The next and final survey prompted for each epoch is the stimulus description survey, shown in Supplementary Figure 6. Users are allowed to read these descriptors in the instructional introduction and to practice answering them with the joystick while immersed in the VR headset. The participants utilize the joystick to move between descriptors and the button on the joystick to toggle each descriptor box on/off: toggle on turns it green, notifying selection of word, and toggle off turns it grey (default color), notifying of deselection of word. Users are allowed to select "NO SENSATION" when finished if none are perceived; otherwise, after choosing appropriate descriptors, they select "FINISHED". There is no time limit on this survey; the next epoch will not begin until this final stimulus description survey is completed. This survey with descriptors was adapted from Graczyk et al. (2022) who utilized it in peripheral nerve stimulation and created it based on previous studies of language associated with both artificial and natural somatosensation (Graczyk et al., 2022).

2.3.7 Auditory stimuli

Two auditory stimulus paradigms are used across the experimental sessions to provide standardized probes of neural responsiveness, with each paradigm selected to match the temporal characteristics of the corresponding measurement method. In Sessions 1 through 3, a brief auditory stimulus is used to elicit short-latency event related potentials measured with EEG. In Sessions 4 through 5, a longer duration auditory stimulus is used to evoke a sustained response suitable for fNIRS, whose hemodynamic signal develops over a slower timescale.

2.3.7.1 Auditory stimulus 1 (sessions 1–3)

During the first three sessions, auditory stimuli are presented to elicit auditory evoked potentials (AEPs), specifically targeting the N1-P2 peak-to-peak amplitude. The stimulus consists of a 1,000 Hz pure tone with an 80 ms plateau and 10 ms linear rise/fall times, presented at 62 dB SPL (Lightfoot, 2016, n.d.). Each trial consists of a 100 ms baseline, 100 ms tone, and 400 ms post-tone interval, followed by a randomized interstimulus interval (ISI) of 0.9–1.1 s (Lightfoot, n.d.). Stimuli are presented during the 30 s auditory stimulation portion of the 90 s experimental epochs, resulting in an average of ~20 presentations per epoch (variability due to randomized ISIs). Recordings are obtained simultaneously from two EEG channels, with non-inverting electrodes positioned at Cz and Pz according to the international 10–20 system and referenced to a common contralateral mastoid electrode.

2.3.7.2 Auditory stimulus 2 (sessions 4–5)

In the final two sessions, a sustained auditory stimulus is used to measure cortical hemodynamic responses with functional near-infrared spectroscopy (fNIRS). The stimulus consists of a 1,000 Hz pure tone with 10 ms linear rise/fall times, presented continuously for 30 s at 62 dB SPL during the stimulation portion of each epoch. This is followed by 30 s of silence, a 30 s pause, and a variable randomized delay of 0–10 s to reduce physiological coupling, such as Mayer waves, and participant predictability. Each auditory stimulation is repeated 15 times for each stimulation parameter setting. fNIRS responses are recorded from eight optodes (C6, T8, CP4, CP6, TP8, P4, P6, P8), corresponding to regions overlying the right temporal and parietal cortex.

2.4 Protocol analytics and outcomes

The following subsections describe the physiologic signals that are collected from study participants and how they are analyzed.

2.4.1 ECG

The raw ECG signal is first preprocessed to remove noise, such as muscle artifacts and baseline wander, using a bandpass zero-phase Butterworth filter (0.5–40 Hz). Then, an R-peak detection algorithm is applied to identify the R-peaks. The following metrics are derived from this:

- *HR (bpm)*: the reciprocal time between consecutive heart beats multiplied by 60, serving as the basis for all HRV analyse.s

- *RMSSD (ms):* (Root Mean Square of Successive Differences): Indicates short-term components of HRV, sensitive to parasympathetic (vagal) activity, and one of the only HRV metrics validated to maintain integrity at such short time windows of 30 s (Shaffer and Ginsberg, 2017).

2.4.2 NIBP

The raw non-invasive blood pressure (NIBP) is recorded and has self-calibration for dynamic changes; however, its baseline scalar blood pressure needs to be calibrated with a brachial cuff measurement at the beginning of testing. Thus, in post processing, the systolic (SBP) and diastolic blood pressure (DBP) values are scalar shifted based on the offset from the brachial cuff measurements, as per instructions from manufacturer. The following metric is used for this application:

- *SBP (mmHg)*: Systolic blood pressure (SBP) represents the peak arterial pressure generated during ventricular contraction. Cervical vagus nerve stimulation can modulate cardiovascular function with changes in arterial pressure (Ahmed et al., 2026).

Similarly, some studies have reported reductions in SBP following taVNS (Nagai et al., 2025; Leite Souza et al., 2026). Therefore, changes in SBP are evaluated as a potential indicator of stimulation evoked autonomic modulation.

2.4.3 EGG

To isolate the gastric slow wave, we apply a zero-phase Butterworth lowpass with a lowpass cutoff of 0.15 Hz, related to around a cutoff of 9 cycles per minute (cpm). From this we calculate the following metric:

- *EGG Amplitude (mV)*: Root-mean-square (RMS) amplitude of the filtered EGG signal calculated over each 30 s analysis window. EGG RMS amplitude was calculated separately for the pre-stimulation baseline and stimulation periods, and the stimulation-associated change was calculated as the difference between the stimulation and pre-stimulation values. It is a representation of strength or regularity of the gastric slow wave, which is the rhythmic electrical activity of the stomach muscles.

2.4.4 GSR

The signal is smoothed using a zero-phase Butterworth lowpass filter (cutoff of 1 Hz) to separate the slow-moving, tonic component (Skin Conductance Level (SCL)) from the fast, phasic responses. Then, a median filter with a time window of 500 ms, followed by a mean filter with a time window of 1000 ms is used to filter rapid appearing movement and contact artifacts. From this remaining signal we calculate the following metric:

- *Skin Conductance Level (μS)*: The tonic, or baseline, level of skin conductance, thought to be a representation of a person's general level of physiological arousal reflecting stress, emotion, and relation. (McCleary, 1950)

2.4.5 EEG

EEG signals were down sampled from 10 kHz to 500 Hz for analysis, median centered, and filtered using a 60-Hz notch filter followed by bandpass filtering. A 0.5–80 Hz band was used for broadband and spectral analyses, while a 0.1–30 Hz band was used for auditory event-related potential (ERP) analysis. Continuous signal segments were screened for large-amplitude artifacts, with samples exceeding ± 250 μV flagged as artifacts for period-level analyses. For auditory ERP analysis, sound-triggered EEG epochs spanning −100 to 500 ms relative to tone onset were extracted and baseline corrected using the −100 to 0 ms pre-tone interval. Accepted tone-locked trials were pooled across all five stimulation repeats for each stimulus level. The pooled ERP was calculated as the median waveform across accepted trials and subsequently smoothed using a 10-ms Gaussian window. N1 and P2 amplitudes were identified within prespecified latency windows of 75–150 ms and 150–250 ms, respectively, and the N1-P2 peak-to-peak amplitude was calculated as the difference between the P2 and N1 amplitudes. Analyses were performed independently for Cz and Pz, with Cz used for the primary N1-P2 outcome.

- *N1-P2 Peak-to-Peak Amplitude (μV)*: The N1-P2 complex originates from multiple generators within the auditory cortex in response to sound. The amplitude of this complex reflects synchronous neural activation of structures in response to sounds, allowing a robust measurement of auditory cortex involvement and activity (Tremblay et al., 2001). Increases in central noradrenaline, as expected with taVNS, has been shown to increase signal to noise ratio in the auditory cortex, which should be reflected by increases in this metric (Ikeda et al., 2015).

2.4.6 fNIRS

The raw fNIRS signal is an optical signal that measures the intensity of near-infrared light at different wavelengths. The finite impulse response model analysis protocol from Luke et al. (2021) was followed for analyzing these signals (Luke et al., 2021).

- *Peak Hemodynamic Response (μM)*: This metric represents the peak value in the wave of hemodynamic change caused by increased oxygenated hemoglobin in brain regions from increased blood flow, regarded an indicator of increased neural activity. (Yücel et al., 2017).

2.4.7 Virtual reality

The raw pupil diameter data is smoothed with a median filter with a time window of 500 ms to reduce fluctuations caused by eye movements and blinks.

- *Pupil Diameter (mm)*: The diameter of the pupil, known to be modulated by the Locus coeruleus noradrenaline (LC-NA) system, of which the LC-NA is often a target of interest in taVNS (Burger et al., 2020).

2.4.8 Survey

The comfort survey data is continuously recorded throughout the stimulation period, with values in the range of −2 (Very uncomfortable) to + 2 (Very comfortable). The data is averaged across the stimulation period in an epoch to get an average score. Other metrics can be derived due to the continuous nature of the comfort survey during stimulation such as peak comfort, peak discomfort, stability in rating, as well as incorporation of the perception survey metrics such as variability in perception. For the purposes of this article and demonstration only average comfort rating is used.

- *Comfort rating (n.u.)*: a subjective metric, that captures a user's perceived level of comfort or discomfort with stimulation.

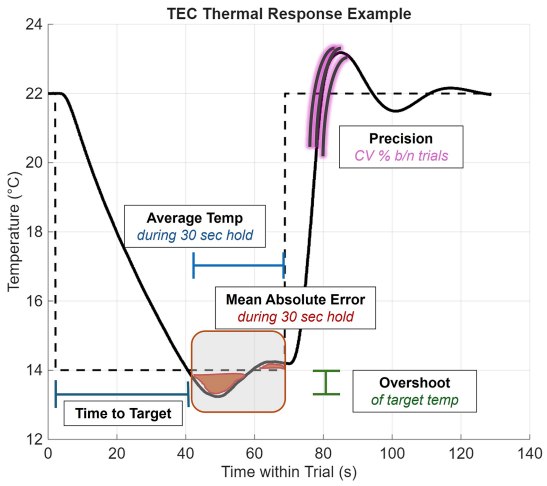

FIGURE 10
Representative thermal response and performance metrics for the TEC-based thermode. The dashed black trace represents the programmed target temperature profile, and the solid black trace represents the measured thermode temperature. After an initial baseline period at 22 °C, the thermode was commanded to heat or cool to a target (14 °C in this example) and held for 30 s before returning to baseline. Annotated regions illustrate the primary performance metrics used for evaluation, including time to target, average hold temperature, mean absolute error during the hold period, overshoot, and trial-to-trial precision. Full metric definitions are provided in section 2.2.2.1.

3 Results

3.1 Vibrotactile stimulator evaluation

The custom vibrotactile stimulator exhibited a voltage dependent response in both vibration acceleration and dominant frequency as shown in Figure 2. Beyond an onset threshold of 0.7 V, the dominant vibration frequency increased continuously with applied voltage, reaching a maximum of 288.7 ± 11.2 Hz at ~3.6 V (Figure 2). Over this operating range, the acceleration response also increased, peaking at 0.37 ± 0.10 g for peak acceleration and 0.15 ± 0.08 g for RMS acceleration near 2.2 V (Figure 2). Across repeated trials ($n = 10$), the device had an average standard deviations of ±13.8 Hz for frequency and ± 0.05 g for peak acceleration. Overall, between 2 and 3 V of applied voltage (corresponding to peak 200 Hz and 250 Hz), more variability occurred in the observed frequencies trial to trial. In addition, peak acceleration showed the greatest variability between 2 and 3 V. Overall, these characterization results demonstrate that the stimulator achieves controllable frequency selection alongside predictable force generation given a graded input voltage to the device.

3.2 Thermal stimulator evaluation

A representative thermal response is shown in Figure 10, illustrating the cooling transition, 30-s target hold period, return to baseline, and the extracted performance metrics. The thermode was characterized across a range of target temperatures spanning cooling and heating conditions relative to room temperature. The relationship between target and measured hold temperature was near linear across the full range, with an overall RMSE of 0.423 °C (Figure 5). Mean absolute error during the hold period remained below approximately 0.96 °C ± 0.53 on average, with the lowest errors observed near room temperature and modestly larger errors at higher target temperatures. Trial-to-trial precision was also stable across the tested range with an average CV of 3.15% ± 0.99 and a corresponding mean between-trial standard deviation of 0.035 °C ± 0.034. Dynamic response depended on the magnitude and direction of the temperature change. Time to target was shortest for temperatures near room temperature and increased as target temperatures deviated farther from ambient, particularly for cooling targets. Overshoot was minimal near and below room temperature but increased for higher heating targets, average of 0.31 °C ± 0.01 at and below room temperature and 2.67 °C ± 0.74 above room temperature. Across all temperatures overshoot was approximately 1.94 °C ± 1.27. Heating/cooling rate also varied with target temperature, with the highest rates observed near the transition above room temperature and lower rates at more extreme target temperatures. The rates in Figure 10 were the maximum achievable heating and cooling rates varied with target temperature. These measurements characterize the dynamic limits of the thermode and are distinct from the controlled target ramp rate of 0.5 °C/s specified for the planned participant protocol. During future participant testing, the same closed-loop temperature control mode will be used with the copper thermode tip in contact with the cymba concha. Temperature feedback will be obtained directly at the thermode tip to regulate the programmed thermal trajectory during stimulation. Together, these results indicate that the thermode provided accurate and repeatable temperature control across the tested range, while dynamic response characteristics varied predictably as a function of target temperature.

3.3 Participant example—data collection

Figure 11 shows a representative TEMPO-taVNS participant with simultaneous physiological recording and auricular vibrotactile stimulation. The recording configuration incorporated PPG, ECG, EGG, GSR, EEG at Cz and Pz, continuous blood-pressure monitoring, digital event recording, together with a wrist mounted unit, virtual reality headset, and response joystick. The vibrotactile stimulator was secured to the external ear and positioned over the cymba conchae, allowing stimulation to be delivered while the participant remained connected to the complete recording and task-presentation system.

Representative recordings from a 133 Hz vibrotactile stimulation epoch are shown in Figure 12. They demonstrate the synchronized acquisition of the physiological signals, stimulation timing, and auditory cue events. All channels were temporally aligned to stimulation onset, with the 30 s stimulation interval and the onset of each of the auditory cues captured by the digital event channel. Continuous systolic and diastolic blood pressure measurements were also recorded throughout the epoch. Together, this example demonstrates the ability of the system to coordinate auricular vibrotactile stimulation, the auditory event presentation, and concurrent multimodal physiological data collection within a single experimental session.

3.4 Participant example—analysis pipeline utilization

The analysis pipeline segmented each stimulus presentation into a 30 s pre-stimulation baseline and a corresponding 30 s stimulation period, all referenced to the Unix timestamped stimulation epoch onsets across devices. Signal specific features were then calculated for each interval, examples include mean heart rate, RMSSD, EGG



FIGURE 11
Experimental setup and placement of the auricular vibrotactile stimulator. **(A)** Participant connected to the recording and stimulation system, including the electrode leads, wrist mounted unit, virtual reality headset, and response joystick held in the left hand. **(B)** Close up of the vibrotactile stimulator secured to the participant's ear and positioned over the cymba conchae.

amplitude, and pupil diameter (Figure 13). Within epoch comparisons enabled visualization of the transition from baseline to stimulation for each repeated presentation, while subtraction of the baseline value from the stimulation value produced a delta change score for each outcome. The resulting change score distributions characterized both the direction and variability of the physiological responses across the nine stimulus settings and provided baseline normalized measures for subsequent participant specific modeling.

The pipeline also processed the participant's perceptual and experiential responses to each stimulus presentation (Figure 14). Comfort ratings summarized the participant's comfort throughout each 30 s stimulation period, and ordinal perceived intensity ratings quantified the perceived strength of each stimulus. Qualitative sensation descriptors were collected across repeated presentations to determine the proportion of trials in which each descriptor was reported at each stimulus level. Together, these measures characterized the tolerability, perceptibility, and subjective qualities of the stimulation across the tested vibrotactile taVNS frequencies.

This representative example demonstrates the use of the custom analysis pipeline to transform synchronized physiological recordings and participant reported responses into stimulus level outcome measures. The resulting objective and subjective features were subsequently used as inputs to the multi-objective Pareto optimization framework. These results illustrate the operation of the analysis workflow and its ability to preserve within-participant response variability.

3.5 Participant example—Pareto-optimized stimulus parameters

In the representative participant, Gaussian process regression produced outcome specific frequency response models for each of the eight physiological and subjective variables included in the multi-objective optimization (Figure 15). The Pareto optimization identified a continuous recommended frequency of 62.99 Hz, with 60 Hz selected when the recommendation was restricted to the frequencies tested experimentally. Thus, the participant specific modeling pipeline generated a continuous solution that closely corresponded to an available experimental setting. These findings provide a demonstration that the system can integrate multiple potentially competing response measures and return an implementable stimulation recommendation; they are not intended to establish 60 Hz as an optimal stimulation frequency or to demonstrate the reliability of the selected parameter across sessions.

4 Discussion

Research in taVNS has been exponentially growing over the last 15 years, with the number of taVNS publications in 2012 jumping from 1 to 112 in 2023 (Fan et al., 2024). This growth has been accompanied by early regulatory and commercial translation of taVNS devices, including the EU-MDR Class IIa tVNS® system developed from the Cerbomed NEMOS platform, indicated in Europe for depression, epilepsy, migraine, and Prader–Willi syndrome, and Spark Biomedical's FDA-cleared Sparrow Ascent, indicated as an aid for reducing opioid-withdrawal symptoms (Spark Biomedical, Inc., 2021; tVNS Technologies GmbH, 2025). Nevertheless, substantial heterogeneity in stimulation modalities, dosing, neural target engagement, and physiological outcome measures continues to impede standardization, underscoring the need for flexible and individualized experimental frameworks such as the approach described in this study.

Here, we present TEMPO-taVNS (Thermal, Electrical, and Mechanical Parameter Optimization for taVNS), an integrated experimental platform for the systematic characterization and individualized optimization of non-electrical transcutaneous auricular vagus nerve stimulation. The platform combines a custom vibrotactile and bidirectional thermal stimulator with the synchronized acquisition of multimodal physiological signals and participant reported responses. We characterized the output properties and performance of both stimulators, developed an analysis pipeline to synchronize stimulation events and quantify evoked responses across recording modalities, and incorporated the resulting features into a multi-objective Pareto optimization framework. This framework enables stimulation parameters to be evaluated and tuned at the individual level according to multiple, potentially competing physiological and subjective outcomes rather than a single predefined endpoint. Collectively, these components

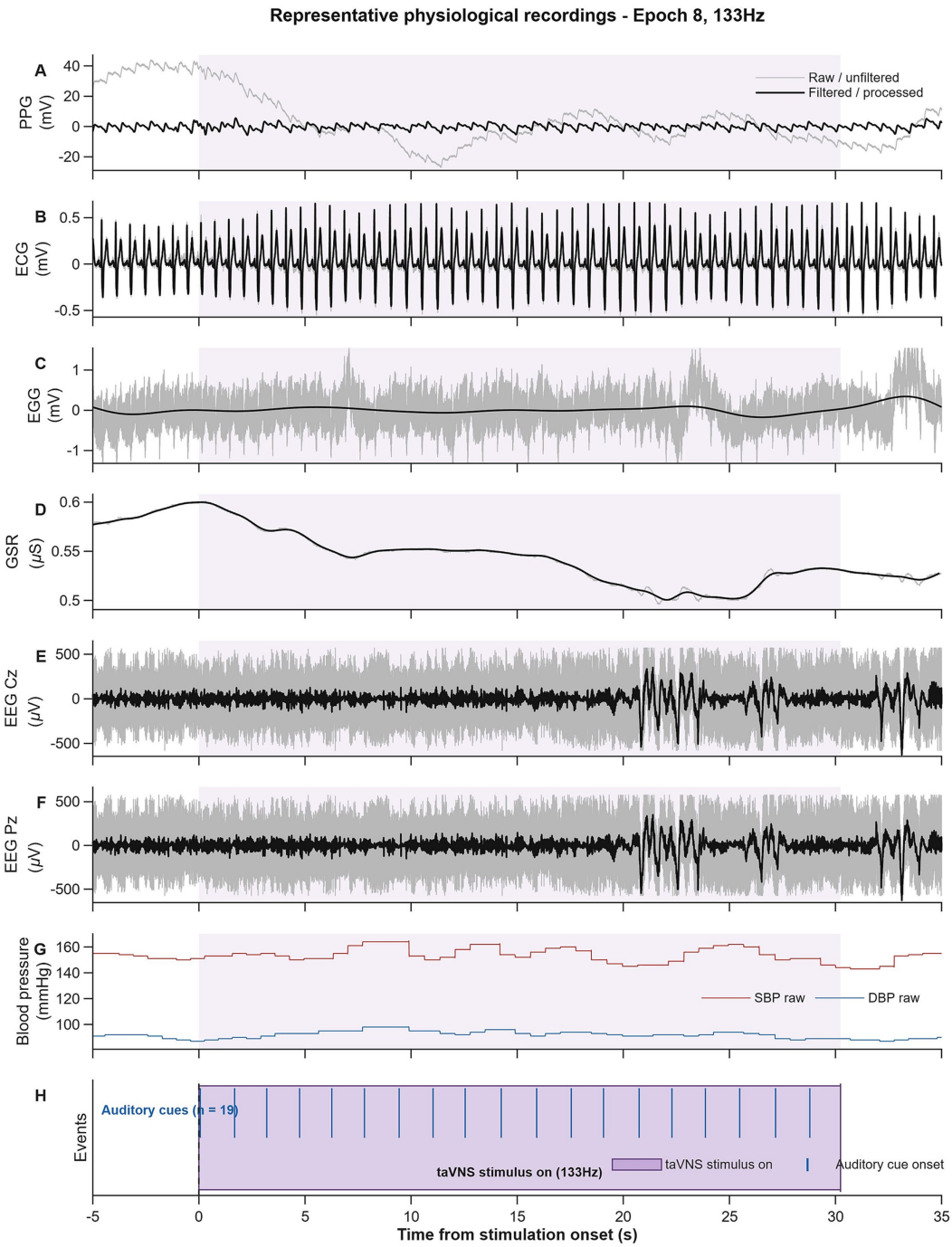

FIGURE 12
Representative raw and processed physiological recordings during auricular vibrotactile stimulation. Data from a single participant are shown for an example 133-Hz stimulation epoch (Epoch 8), with all signals aligned to stimulation onset at t = 0 s. Traces are presented from top to bottom as follows: **(A)** photoplethysmography (PPG), **(B)** electrocardiography (ECG), **(C)** electrogastrography (EGG), **(D)** galvanic skin response (GSR), **(E)** electroencephalography (EEG) recorded at Cz, **(F)** EEG recorded at Pz, **(G)** continuous systolic (SBP) and diastolic (DBP) blood pressure, and **(H)** digital event markers. In panels **(A)**–**(F)**, raw or unfiltered signals are shown in light gray and filtered or processed signals are shown in black. In panel **(G)**, systolic and diastolic pressure are shown in red and blue. The shaded interval from 0 to 30 s denotes the 133-Hz stimulation period. Blue vertical markers in panel **(H)** indicate the onset of the 19 auditory cues presented during the stimulation epoch.

establish a modular approach for systematic parameter exploration and data driven personalization of non-electrical taVNS.

4.1 Non-electrical taVNS

Relatively few studies have investigated non-electrical taVNS using vibrotactile stimulation, and, to our knowledge, dedicated hardware designed for thermal taVNS has not previously been reported. Existing vibrotactile studies have also generally employed a single stimulation frequency or a narrowly defined parameter set, limiting the ability to determine how stimulation characteristics influence the resulting physiological response. Only in Donovan et al. (2025) were more than a single frequency tested, 2, 6, 12, 20, and 40 Hz (Donovan et al., 2025). Nevertheless, prior vibrotactile studies have

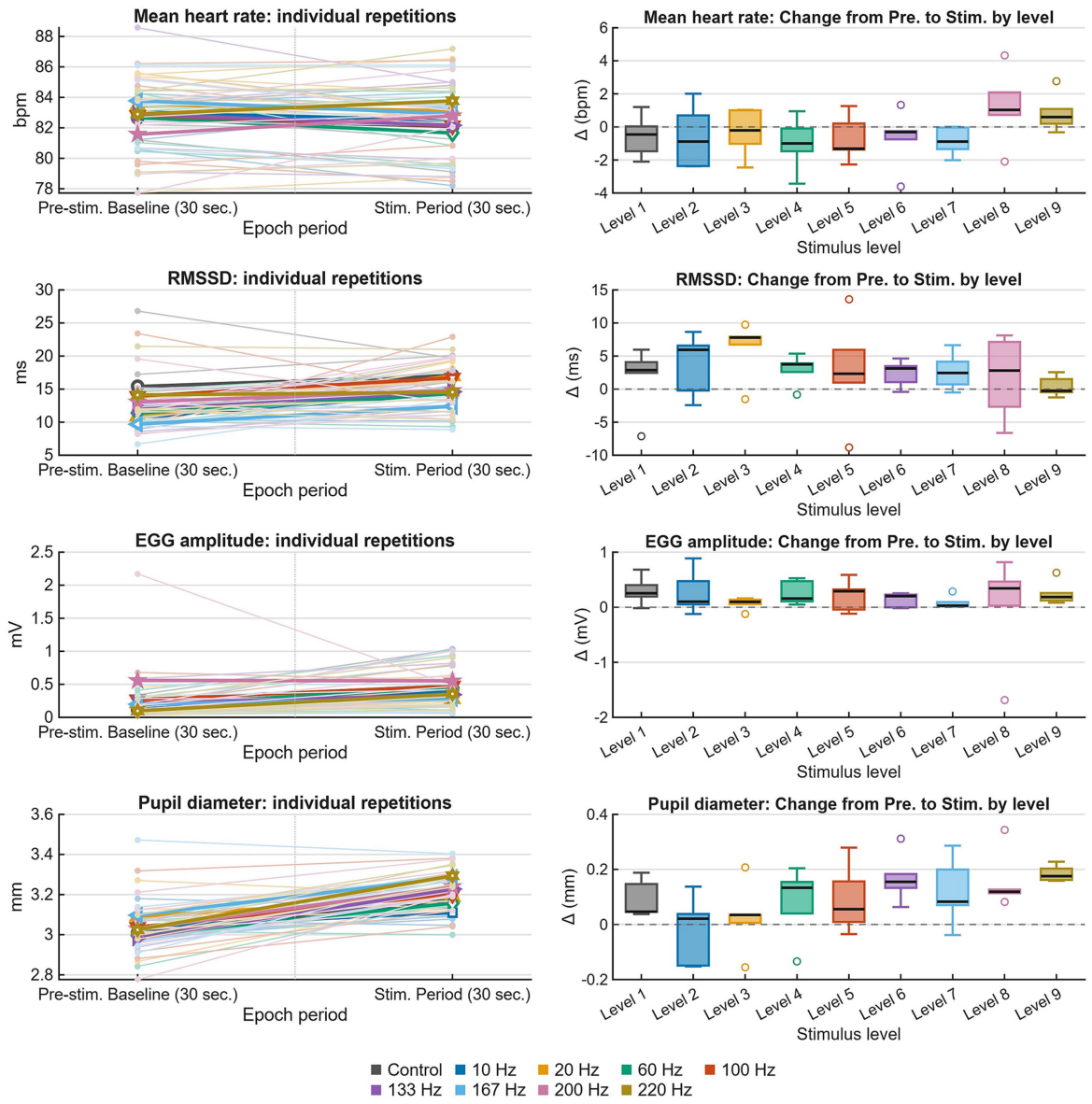

FIGURE 13
Representative within epoch physiological responses across auricular vibrotactile stimulation levels. Data from a representative participant is shown for mean heart rate, the root mean square of successive differences between (RMSSD), electrogastrographic (EGG) amplitude, and pupil diameter, arranged from top to bottom. Left panels compare values obtained during the 30 s pre-stimulation baseline and the subsequent 30 s stimulation period. Thin, semi-transparent lines connect measurements from individual repetitions, whereas thicker colored lines and markers indicate the mean response for each stimulus level. Right panels show the distributions of change scores for each level, calculated as the stimulation period value minus the corresponding pre-stimulation baseline value (Δ = stimulation − baseline). Boxes represent the interquartile range with the median indicated by the horizontal line, whiskers show the non-outlier range, and open circles denote outliers. The horizontal dashed line indicates no change from baseline. Stimulus levels 1–9 correspond to control, 10, 20, 60, 100, 133, 167, 200, and 220 Hz, respectively, as indicated by the color legend.

typically evaluated stimulation within the context of a specific task or a limited outcome domain, such as EEG activity or task performance. Although these focused designs are appropriate for addressing application specific hypotheses, they provide limited information regarding the broader pattern of central and peripheral physiological responses associated with stimulation. The present framework extends this work by enabling individualized, structured exploration of vibrotactile and thermal stimulation parameters while simultaneously measuring a broad range of physiological and perceptual outcomes. This distinction is particularly important for individualized stimulation because the parameter setting that produces the largest response in one outcome may not produce the most desirable response in another.

4.2 Limitations

The experimental configuration used in the present study was intentionally comprehensive and consequently relied on several high cost research grade systems, including the VR headset and ADInstruments acquisition hardware. The cost of this equipment may limit direct replication of the complete setup; however, the broader framework is not dependent on any single recording platform and can be scaled according to the scientific question, available resources, and outcomes of interest. The custom stimulation hardware is comparatively inexpensive, and much of the experimental control, synchronization, and analysis pipeline is software based or can be implemented

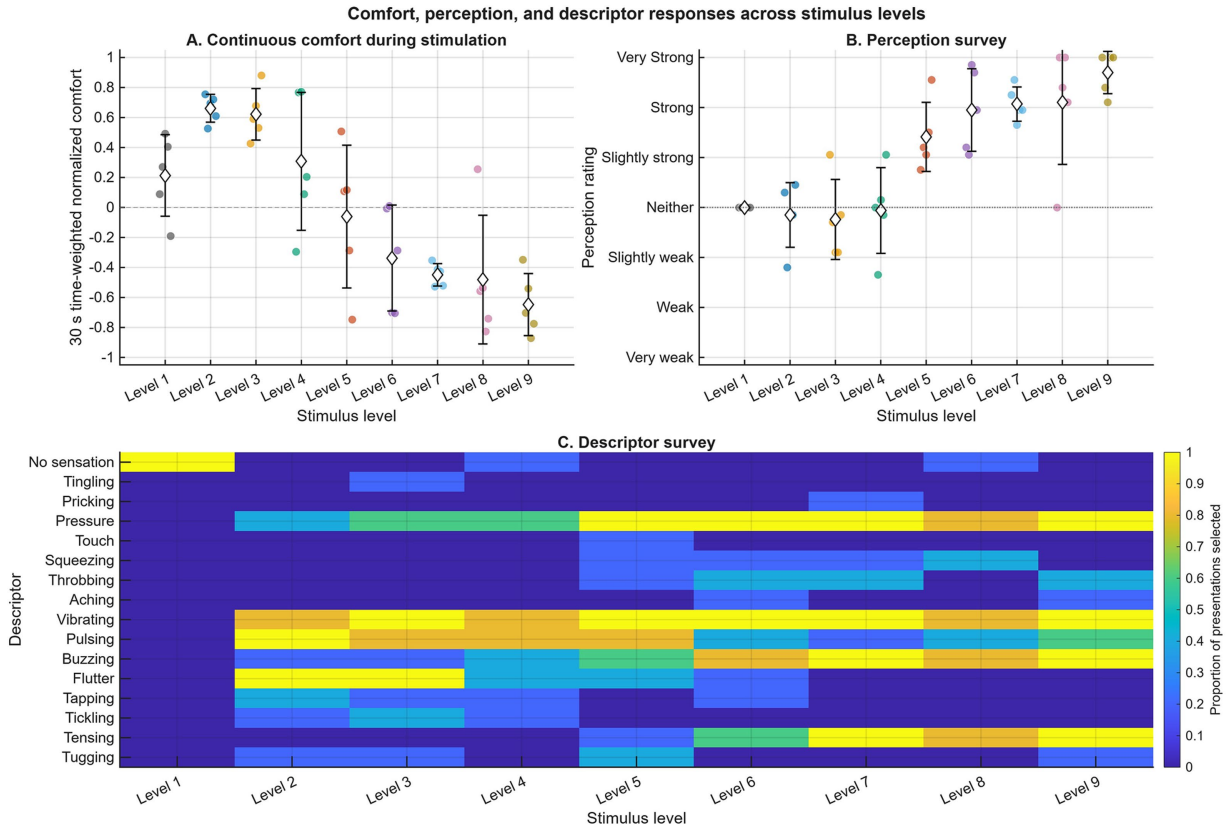

FIGURE 14
Comfort, perception, and qualitative sensation descriptors across vibrotactile stimulus levels. **(A)** Thirty second time weighted normalized comfort scores for each of nine stimulus levels. Colored circles represent individual presentation ratings, open diamonds indicate mean ratings, and black error bars represent ± SD. The dashed reference line denotes neutral comfort (0), with positive and negative values indicating greater and lower comfort, respectively. **(B)** Perceived stimulus intensity at each level, rated on a seven-point ordinal scale ranging from "very weak" to "very strong." Colored circles show individual ratings, open diamonds indicate mean ratings, and error bars represent ± SEM. The dashed line denotes the neutral category ("neither"). **(C)** Heat map of the qualitative descriptors selected for each stimulus level. Cell color and overlaid percentages indicate the proportion of presentations for which each descriptor was selected, ranging from 0 (dark blue) to 1 (yellow).

using freely available tools. For example, a study focused primarily on heart rate could replace the full cardiovascular recording system with a lower cost photoplethysmography sensor, whereas studies focused on cortical or gastrointestinal responses could retain only the relevant EEG or EGG channels. Similarly, the experimental software can be adapted to interface with alternative stimulation devices as they become available. To our knowledge, however, comparable thermal and vibrotactile stimulators developed specifically for systematic non-electrical auricular stimulation are not currently available, only these described methods.

Another limitation is that when interpreting the cardiac findings in this system, the stimulated nerve cannot be identified with certainty. Although the auricular target was selected to engage the auricular branch of the vagus nerve (ABVN), the sensory innervation of the external ear is heterogeneous and remains incompletely characterized; consequently, stimulation at a nominal vagal target cannot be assumed to activate the ABVN exclusively. Adjacent trigeminal afferents, including the auriculotemporal nerve, or other somatosensory–autonomic reflex pathways may therefore have contributed to the observed changes in heart rate. Supporting this possibility, Perçin et al. (2026) found that both transcutaneous auricular vagus nerve stimulation and transcutaneous auricular trigeminal nerve stimulation decreased heart rate and increased RMSSD, although taVNS produced a greater increase in RMSSD and reduced systolic blood pressure, whereas trigeminal stimulation did not (Perçin et al., 2026). Although that study used electrical stimulation, the shared cardiac responses indicate that reductions in heart rate are not necessarily specific to ABVN activation. The present findings should therefore be interpreted as evidence of auricular autonomic modulation consistent with ABVN engagement, rather than definitive evidence of selective ABVN activation.

Furthermore, optimization of the prespecified multivariate response profile should be distinguished from mechanistic validation of ABVN engagement. The Pareto framework identifies stimulation parameters that best balance the selected physiological and perceptual objectives, but the specificity of those outcomes to vagal activation is not established by the optimization itself. Accordingly, an optimized parameter should be considered a candidate setting for subsequent physiological and mechanistic validation rather than evidence of selective ABVN recruitment.

An additional limitation for the vibrotactile methods is that stimulation frequency is not manipulated independently of other mechanical characteristics of the stimulus. As shown by the device characterization, changes in motor operating conditions were accompanied by changes in vibration acceleration. Accordingly, physiological responses should be interpreted as responses to distinct vibrotactile stimulation conditions rather than effects attributable exclusively to vibration frequency. Additionally, although the 0-Hz

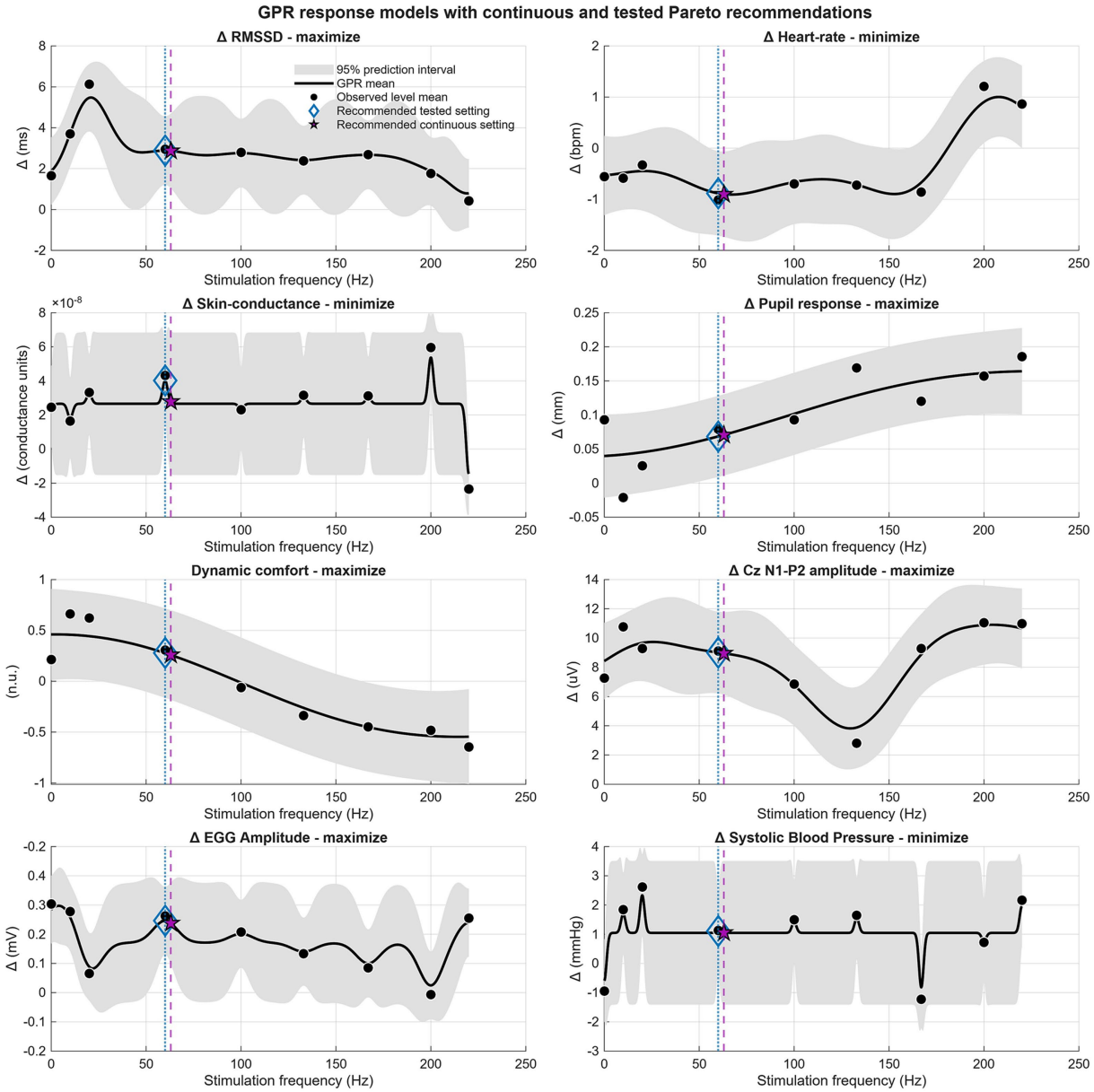

FIGURE 15
Gaussian process regression (GPR) models of physiological and perceptual responses across vibrotactile stimulation frequencies. GPR models are shown for eight response variables included in the multi-objective optimization. From top left to bottom right, the modeled outcomes are the change in the root mean square of successive differences (RMSSD; maximize), heart rate (minimize), skin conductance (minimize), pupil response (maximize), dynamic comfort (maximize), Cz N1-P2 amplitude (maximize), electrogastrography (EGG) amplitude (maximize), and systolic blood pressure (SBP; minimize). Black curves represent the GPR posterior mean, gray shaded regions indicate the 95% prediction intervals, and black circles denote the observed mean response at each experimentally tested frequency. The magenta star and vertical magenta line indicate the Pareto-recommended continuous frequency of 62.99 Hz, whereas the blue diamond and vertical blue dashed line indicate the recommended experimentally tested frequency of 60 Hz.

control condition retained the same auditory stimulation, VR presentation, continuous comfort reporting, and survey procedures as the active conditions, these concurrent sensory and behavioral tasks may themselves influence autonomic or central responses. Participants remained supine to reduce gross movement, and respiration was recorded but was not incorporated as a covariate in the present analysis. Moreover, stimulation of the cymba concha does not establish selective recruitment of the ABVN, as responses may reflect activation of other local sensory afferents or nonspecific sensory and perceptual effects. Accordingly, the present physiological findings demonstrate responses associated with the overall stimulation condition rather than independent evidence of ABVN engagement.

A further limitation is the duration and participant burden associated with the proposed protocols, which comprise approximately five experimental sessions lasting more than one hour each. This design was intentionally expansive because the effective parameter spaces for vibrotactile and thermal auricular stimulation have not yet been established, and the present framework was developed to examine a broad range of stimulation conditions and physiological outcomes. It should therefore be viewed as a discovery-oriented methodology rather than a finalized clinical or experimental workflow. Future studies may

identify a narrower range of effective parameters, a smaller subset of informative outcome measures, or more efficient adaptive sampling strategies which could substantially reduce the number and duration of required sessions. In addition, the current framework was designed to characterize acute responses to taVNS and does not address the effects of repeated or chronic stimulation, including possible habituation, cumulative physiological changes, or differences between acute and long-term therapeutic efficacy. Given the novelty of these stimulation modalities, establishing their immediate physiological effects represents an appropriate first step before progressing to longitudinal protocols. Nevertheless, acute responses should not be assumed to predict the efficacy, tolerability, or durability of effects during chronic use, and these questions will require dedicated future investigation.

4.3 Potential effects of taVNS on perceptual thresholds

An important consideration is whether taVNS itself alters the perceptual thresholds used to calibrate thermal stimulation in the manner we performed. A stimulation related shift in warm/cold thresholds or hot/cold pain thresholds could introduce an order-dependent confound when thermal modalities are tested sequentially and could complicate the interpretation of evoked responses. This specific consideration remains sparsely studied; however, available evidence is reassuring for acute stimulation. Gonzalez et al. (2026) compared sensory thresholds between changing duty cycles of taVNS as well as monophasic vs. biphasic taVNS. They tested hot and cold pain thresholds as well as mechanical pain thresholds before and after taVNS in the two crossover studies and reported predominantly small to negligible changes in quantitative sensory testing (Gonzalez et al., 2026). Changes in static thermal measures did not differ between the active taVNS parameter conditions, whereas wind-up, a dynamic measure of nociceptive temporal summation, differed between monophasic and biphasic stimulation (Gonzalez et al., 2026). This subject, while not widely studied, has current evidence supporting that the taVNS itself should not shift thermal thresholds in any meaningful manner. However, it should be considered that if vibrotactile thresholds are measured there is potential alteration there.

4.4 Interpretation of the *n* = 1 demonstration

The single participant demonstration should be interpreted as an illustrative proof of concept rather than evidence of efficacy. The primary purpose of the present manuscript is to establish the feasibility of the integrated methodology and demonstrate that stimulation can be delivered while synchronized multimodal physiological and subjective responses are acquired, processed, and incorporated into the individualized optimization framework. Accordingly, these results do not establish the relative efficacy of vibrotactile stimulation, thermal stimulation, or conventional electrical taVNS. Furthermore, the participant specific parameter identified by the optimization should be interpreted as an unvalidated candidate rather than an established optimal stimulation setting. The recommendation was derived from repeated measurements obtained within a single experimental session and was not subsequently evaluated in an independent validation session. Furthermore, the sensitivity of the recommendation to trial-to-trial variability and selection of individual outcomes was not systematically evaluated in this proof-of-concept demonstration. Future studies should assess the stability of candidate parameters across repeated measurements and alternative outcome sets and prospectively test the selected parameters in independent sessions. Whether the complete workflow produces reliable, generalizable, and clinically informative measures of target engagement will require evaluation in an adequately powered pilot study, likely followed by replication in an independent sample. However, the demonstrated performance of the individual platform components provides a foundation for future studies directly comparing thermal, vibrotactile, and conventional electrical stimulation using simultaneous multimodal physiological characterization. A properly powered pilot study will be required to directly evaluate these stimulation modalities and quantify the reliability, sensitivity, and between-participant variability of the methodology.

4.5 Application-specific outcome selection and future directions

An important direction for future research will be to determine whether the complete multimodal outcome set is necessary for every application or whether a more focused, indication specific set of endpoints would be preferable. The framework presented here is intentionally broad measuring cortical, cardiovascular, gastrointestinal, and other autonomic and cholinergic responses. This broad measurement set is valuable during early mechanistic investigations where the relevant physiological markers of target engagement may not yet be known, as both thermal and vibrotactile stimulation are still in their infancy. In later stage or application specific studies, limiting the primary outcomes or measures could prove useful. It could reduce participant burden and statistical multiplicity while improving power and interpretability. For example, in studies of tinnitus or taVNS paired with bimodal auditory stimulation, EEG derived measures of auditory cortical engagement or plasticity may be more directly relevant to the proposed therapeutic mechanism than gastrointestinal or broad autonomic outcomes. These latter measures could therefore be treated as secondary endpoints or omitted for personalization or optimization when they do not address the principal mechanistic question. Conversely, studies targeting gastrointestinal, cardiovascular, or other autonomic disorders may prioritize gastrointestinal physiology, heart rate and heart rate variability, while retaining EEG as a secondary measure of central target engagement. Outcome selection potentially may be guided by the physiological pathway and clinical application being targeted.

Additionally, beyond single-modality delivery, the TEMPO-taVNS system architecture supports complex, concurrent combinations of thermal, mechanical, and electrical inputs to the auricular branch. Efficiently mapping and optimizing this expansive multiparametric landscape remains a goal for subsequent studies, where artificial intelligence strategies will be essential to identify synergistic bioelectronic protocols.

Data availability statement

The raw data supporting the conclusions of this article will be made available by the authors, without undue reservation.

Ethics statement

The studies involving humans were approved by Purdue University Institutional Review Board. The studies were conducted in accordance with the local legislation and institutional requirements. The participants provided their written informed consent to participate in this study. Written informed consent was obtained from the individual(s) for the publication of any identifiable images or data included in this article.

Author contributions

DW: Writing – original draft, Methodology, Visualization, Software, Formal analysis, Investigation, Resources, Validation, Data curation, Writing – review & editing, Conceptualization. MS: Project administration, Writing – original draft, Conceptualization, Writing – review & editing, Supervision, Resources. SS: Conceptualization, Project administration, Writing – review & editing, Investigation, Writing – original draft, Supervision. MW: Writing – review & editing, Supervision, Writing – original draft, Project administration, Investigation, Funding acquisition, Conceptualization.

Funding

The author(s) declared that financial support was received for this work and/or its publication. Research supported by NIH 1T32DC016853, T32GM148382, McKinley Educational Initiative, and the Ehlers Danlos Society.

Acknowledgments

We thank P. Zoss for assistance with technical troubleshooting and, together with V. Napadow, for input and feedback on the design and setup of the system. We also thank the Bechtel Innovation Design Center for providing access to on-campus CNC machining capabilities.

Conflict of interest

MW and DW are named inventors on a provisional patent application covering aspects of the methods and system described in this manuscript.

The remaining author(s) declared that this work was conducted in the absence of any commercial or financial relationships that could be construed as a potential conflict of interest.

Generative AI statement

The author(s) declared that Generative AI was used in the creation of this manuscript. During preparation of this manuscript, the authors used ChatGPT Edu with the GPT-5.6 Pro model (OpenAI, San Francisco, CA, USA) to assist with drafting, rewording, and editing portions of the manuscript. ChatGPT with the GPT-5.6 Sol model (OpenAI, San Francisco, CA, USA) was separately used to assist in developing the manuscript title and the acronym "TEMPO-taVNS". All AI-assisted material was critically reviewed, revised, and verified by the authors, who take full responsibility for the final content of the manuscript.

Any alternative text (alt text) provided alongside figures in this article has been generated by Frontiers with the support of artificial intelligence and reasonable efforts have been made to ensure accuracy, including review by the authors wherever possible. If you identify any issues, please contact us.

Publisher's note

All claims expressed in this article are solely those of the authors and do not necessarily represent those of their affiliated organizations, or those of the publisher, the editors and the reviewers. Any product that may be evaluated in this article, or claim that may be made by its manufacturer, is not guaranteed or endorsed by the publisher.

Supplementary material

The Supplementary material for this article can be found online at: https://www.frontiersin.org/articles/10.3389/fnins.2026.1983186/full#supplementary-material

References

Addorisio, M. E., Imperato, G. H., de Vos, A. F., Forti, S., Goldstein, R. S., Pavlov, V. A., et al. (2019). Investigational treatment of rheumatoid arthritis with a vibrotactile device applied to the external ear. *Bioelectron. Med.* 5:4. doi: 10.1186/s42234-019-0020-4

Ahmed, R., Coello, A., Pillutla, A. S., Telwar, G., and Stauss, H. M. (2026). Acute transcutaneous cervical but not auricular vagus nerve stimulation increases alpha wave brain activity and lowers arterial blood pressure. *Am. J. Physiol. Integr. Comp. Physiol.* 330, R49–R59. doi: 10.1152/ajpregu.00219.2025

Antonino, D., Teixeira, A. L., Maia-Lopes, P. M., Souza, M. C., Sabino-Carvalho, J. L., Murray, A. R., et al. (2017). Non-invasive vagus nerve stimulation acutely improves spontaneous cardiac baroreflex sensitivity in healthy young men: a randomized placebo-controlled trial. *Brain Stimul.* 10, 875–881. doi: 10.1016/j.brs.2017.05.006.

Austelle, C. W., Sege, C. T., Kahn, A. T., Gregoski, M. J., Taylor, D. L., McTeague, L. M., et al. (2024). Transcutaneous auricular vagus nerve stimulation attenuates early increases in heart rate associated with the cold pressor test. *Neuromodulation* 27, 1227–1233. doi: 10.1016/j.neurom.2023.07.012.

Badran, B. W., Mithoefer, O. J., Summer, C. E., LaBate, N. T., Glusman, C. E., Badran, A. W., et al. (2018). Short trains of transcutaneous auricular vagus nerve stimulation (taVNS) have parameter-specific effects on heart rate. *Brain Stimul.* 11, 699–708. doi: 10.1016/j.brs.2018.04.004.

Bolanowski, S. J., and Verrillo, R. T. (1982). Temperature and criterion effects in a somatosensory subsystem: a neurophysiological and psychophysical study. *J. Neurophysiol.* 48, 836–855. doi: 10.1152/jn.1982.48.3.836.

Burger, A. M., D'Agostini, M., Verkuil, B., and Van Diest, I. (2020). Moving beyond belief: a narrative review of potential biomarkers for transcutaneous vagus nerve stimulation. *Psychophysiology* 57:e13571. doi: 10.1111/psyp.13571.

Butt, M. F., Albusoda, A., Farmer, A. D., and Aziz, Q. (2020). The anatomical basis for transcutaneous auricular vagus nerve stimulation. *J. Anat.* 236, 588–611. doi: 10.1111/joa.13122.

Choinière, L., Guay-Hottin, R., Picard, R., Lajoie, G., Bonizzato, M., and Dancause, N. (2024). Gaussian-process-based Bayesian optimization for neurostimulation interventions in rats. *STAR Protoc.* 5:102885. doi: 10.1016/j.xpro.2024.102885

Dabiri, B., Zeiner, K., Nativel, A., and Kaniusas, E. (2022). Auricular vagus nerve stimulator for closed-loop biofeedback-based operation. *Analog Integr. Circuits Signal Process.* 112, 237–246. doi: 10.1007/s10470-022-02037-8.

Das, J. M., and Breiner, M. J. (2026). *Anatomy, Head and Neck: Auriculotemporal Nerve*. Treasure Island: StatPearls Publishing. Available online at: http://www.ncbi.nlm.nih.gov/books/NBK544240/ (Accessed August 19, 2026).

Deb, K., Pratap, A., Agarwal, S., and Meyarivan, T. (2002). A fast and elitist multiobjective genetic algorithm: NSGA-II. *IEEE Trans. Evol. Comput.* 6:182. doi: 10.1109/4235.996017

Donovan, K. M., Adams, J. D., Park, K. Y., Demarest, P., Tan, G., Willie, J. T., et al. (2025). Vibrotactile auricular vagus nerve stimulation alters limbic system connectivity in humans: a pilot study. *PloS One* 20:e0310917. doi: 10.1371/journal.pone.0310917.

Essick, G., Guest, S., Martinez, E., Chen, C., and Mcglone, F. (2004). Site-dependent and subject-related variations in perioral thermal sensitivity. *Somatosens. Motor Res.* 21, 159–175. doi: 10.1080/08990220400012414.

Fan, S., Yan, L., Zhang, J., Sun, Y., Qian, Y., Wang, M., et al. (2024). Transcutaneous vagus nerve stimulation: a bibliometric study on current research hotspots and status. *Front. Neurosci.* 18:1406135. doi: 10.3389/fnins.2024.1406135.

Frei, M. G., and Osorio, I. (2001). Left vagus nerve stimulation with the Neurocybernetic Prosthesis has complex effects on heart rate and on its variability in humans. *Epilepsia* 42, 1007–1016. doi: 10.1046/j.1528-1157.2001.0420081007.x.

Gonzalez, G., O'Malley, M., Bolanos, J., Taylor, D., McTeague, L. M., Canepa, A., et al. (2026). Participant-centered tolerability of transcutaneous auricular vagus nerve stimulation: insights from two crossover studies. *Bioelectron. Med.* 12:12. doi: 10.1186/s42234-026-00206-y.

Graczyk, E. L., Christie, B. P., He, Q., Tyler, D. J., and Bensmaia, S. J. (2022). Frequency shapes the quality of tactile percepts evoked through electrical stimulation of the nerves. *J. Neurosci.* 42, 2052–2064. doi: 10.1523/JNEUROSCI.1494-21.2021

Gutierrez, V., Coverdell, T., Abbott, S., and Campbell, J. (2023). Disambiguating control of the diving reflex by the nucleus ambiguus. *Physiology* 38:5729637. doi: 10.1152/physiol.2023.38.S1.5729637

Ikeda, M. Z., Jeon, S. D., Cowell, R. A., and Remage-Healey, L. (2015). Norepinephrine modulates coding of complex vocalizations in the songbird auditory cortex independent of local neuroestrogen synthesis. *J. Neurosci.* 35, 9356–9368. doi: 10.1523/JNEUROSCI.4445-14.2015.

ISO 7730:2005 (n.d.). *ISO*. Available online at: https://www.iso.org/standard/39155.html (Accessed August 22, 2025).

Ivanova, Y. M., Pallubinsky, H., Kramer, R., and van Marken Lichtenbelt, W. (2021). The influence of a moderate temperature drift on thermal physiology and perception. *Physiol. Behav.* 229:113257. doi: 10.1016/j.physbeh.2020.113257.

Joshi, A., Kale, S., Chandel, S., and Pal, D. K. (2015). Likert scale: explored and explained. *Br. J. Appl. Sci. Technol.* 7, 396–403. doi: 10.9734/BJAST/2015/14975

Kaniusas, E., Kampusch, S., Tittgemeyer, M., Panetsos, F., Gines, R. F., Papa, M., et al. (2019a). Current directions in the auricular vagus nerve stimulation I—a physiological perspective. *Front. Neurosci.* 13:854. doi: 10.3389/fnins.2019.00854.

Kaniusas, E., Kampusch, S., Tittgemeyer, M., Panetsos, F., Gines, R. F., Papa, M., et al. (2019b). Current directions in the auricular vagus nerve stimulation II—an engineering perspective. *Front. Neurosci.* 13:772. doi: 10.3389/fnins.2019.00772.

Kawai, A., and Tanaka, Y. (2022). "Individual differences in skin vibration characteristics and vibrotactile sensitivity at fingertip," in 2022 IEEE haptics symposium (HAPTICS), Piscataway, NJ, United States: IEEE. 1–6. doi: 10.1109/HAPTICS52432.2022.9765612

Kim, H.-K., Kim, K.-S., and Kim, M.-E. (2013). Influence of test site and baseline temperature on orofacial thermal thresholds. *J. Orofac. Pain* 27, 263–270. doi: 10.11607/jop.1030

Kim, A. Y., Marduy, A., de Melo, P. S., Gianlorenco, A. C., Kim, C. K., Choi, H., et al. (2022). Safety of transcutaneous auricular vagus nerve stimulation (taVNS): a systematic review and meta-analysis. *Sci. Rep.* 12:22055. doi: 10.1038/s41598-022-25864-1.

Krahl, S. E., Senanayake, S. S., and Handforth, A. (2001). Destruction of peripheral C-fibers does not alter subsequent vagus nerve stimulation-induced seizure suppression in rats. *Epilepsia* 42, 586–589. doi: 10.1046/j.1528-1157.2001.09700.x.

Lechner, S. G., and Lewin, G. R. (2013). Hairy sensation. *Physiology* 28, 142–150. doi: 10.1152/physiol.00059.2012

Lee, J.-Y., Stone, E. A., Wakabayashi, H., and Tochihara, Y. (2010). Issues in combining the categorical and visual analog scale for the assessment of perceived thermal sensation: methodological and conceptual considerations. *Appl. Ergon.* 41, 282–290. doi: 10.1016/j.apergo.2009.07.007.

Leite Souza, P. H., Ferrari Corrêa, J. C., Venâncio, B. P., Buzá, L. S., Oliveira da Silva, G., Fregni, F., et al. (2026). Acute effect of transcutaneous auricular vagus nerve stimulation in two different locations on blood pressure and cardiac autonomic modulation in healthy and hypertensive individuals: pilot study of a randomized crossover clinical trial. *Physiother. Res. Int.* 31:e70209. doi: 10.1002/pri.70209

Lemaitre, F., and Schaller, B. J. (2015). "Chapter 15—the trigeminocardiac reflex: a comparison with the diving reflex in humans," in *Trigeminocardiac Reflex*, eds. T. Chowdhury and B. J. Schaller (Boston: Academic Press), 193–206.

Lightfoot, G. (n.d.). *The N1-P2 Cortical Auditory Evoked Potential in Threshold Estimation—Article 851*. AudiologyOnline. Available online at: https://www.audiologyonline.com/articles/n1-p2-cortical-auditory-evoked-851 (Accessed August 25, 2025).

Lightfoot, G. (2016). Summary of the N1-P2 cortical auditory evoked potential to estimate the auditory threshold in adults. *Semin. Hear.* 37, 001–008. doi: 10.1055/s-0035-1570334.

Lithfous, S., Trocmet, L., Pebayle, T., Després, O., and Dufour, A. (2022). Investigating cold Aδ fibers in the 0–40 °C temperature range: a quantitative sensory testing and evoked potentials study. *Clin. Neurophysiol.* 134, 81–87. doi: 10.1016/j.clinph.2021.11.076.

Luke, R., Larson, E. D., Shader, M. J., Innes-Brown, H., Yper, L. V., Lee, A. K. C., et al. (2021). Analysis methods for measuring passive auditory fNIRS responses generated by a block-design paradigm. *NPh* 8:025008. doi: 10.1117/1.NPh.8.2.025008

Luo, M., Wang, Z., Zhang, H., Arens, E., Filingeri, D., Jin, L., et al. (2020). High-density thermal sensitivity maps of the human body. *Build. Environ.* 167:106435. doi: 10.1016/j.buildenv.2019.106435

McCleary, R. A. (1950). The nature of the galvanic skin response. *Psychol. Bull.* 47, 97–117. doi: 10.1037/h0059810

Nagai, M., Rommel, K.-P., Nakano, Y., Tully, P. J., Sible, I. J., Po, S., et al. (2025). Association between non-invasive auricular stimulation and blood pressure lowering: a systematic review and meta-analysis. *Eur. Heart J. Open* 5:oeaf098. doi: 10.1093/ehjopen/oeaf098.

Onishi, Y., Hisato, H., Maeda, S., Minato, Y., Kuwahara-Otani, S., and Yagi, H. (2021). Relationship between lamellar sensory corpuscles distributed along the upper arm's deep arteries and pulsating sensation of blood vessels. *J. Anat.* 239, 101–110. doi: 10.1111/joa.13398.

Panneton, W. M., and Gan, Q. (2020). The mammalian diving response: inroads to its neural control. *Front. Neurosci.* 14:524. doi: 10.3389/fnins.2020.00524.

Perçin, A., Özden, A. V., Yenişehir, S., and Albayrak, H. E. (2026). Autonomic effects of transcutaneous auricular vagus and trigeminal nerve stimulation: a randomized, sham-controlled, and single-blind study. *Neuromodulation Technol. Neural Interface* 29, 588–596. doi: 10.1016/j.neurom.2025.09.312.

Peuker, E. T., and Filler, T. J. (2002). The nerve supply of the human auricle. *Clin. Anat.* 15, 35–37. doi: 10.1002/ca.1089

Redgrave, J., Day, D., Leung, H., Laud, P. J., Ali, A., Lindert, R., et al. (2018). Safety and tolerability of transcutaneous vagus nerve stimulation in humans; a systematic review. *Brain Stimul.* 11, 1225–1238. doi: 10.1016/j.brs.2018.08.010

Safi, S., Ellrich, J., and Neuhuber, W. (2016). Myelinated axons in the auricular branch of the human vagus nerve. *Anat. Rec. (Hoboken)* 299, 1184–1191. doi: 10.1002/ar.23391.

Sato, M. (1961). Response of Pacinian corpuscles to sinusoidal vibration. *J. Physiol.* 159, 391–409. doi: 10.1113/jphysiol.1961.sp006817.

Schmidt, D., Schlee, G., Milani, T. L., and Germano, A. M. C. (2023). Vertical contact forces affect vibration perception in human hairy skin. *PeerJ* 11:e15952. doi: 10.7717/peerj.15952.

Sclocco, R., García, R. G., Kettner, N. W., Fisher, H., Isenburg, K., Makarovsky, M., et al. (2020). Stimulus frequency modulates brainstem response to respiratory-gated transcutaneous auricular vagus nerve stimulation. *Brain Stimul.* 13, 970–978. doi: 10.1016/j.brs.2020.03.011

Sclocco, R., Garcia, R. G., Kettner, N. W., Isenburg, K., Fisher, H. P., Hubbard, C. S., et al. (2019). The influence of respiration on brainstem and cardiovagal response to auricular vagus nerve stimulation: a multimodal ultrahigh-field (7T) fMRI study. *Brain Stimul.* 12, 911–921. doi: 10.1016/j.brs.2019.02.003.

Shaffer, F., and Ginsberg, J. P. (2017). An overview of heart rate variability metrics and norms. *Front. Public Health* 5:258. doi: 10.3389/fpubh.2017.00258.

Spark Biomedical, Inc. (2021). *Sparrow Therapy System*. Silver Spring: Food and Drug Administration. Available online at: https://www.accessdata.fda.gov/scripts/cdrh/cfdocs/cfpmn/pmn.cfm?ID=K201873 (Accessed date is March 26, 2026).

Sperduti, M., Tagliamonte, N. L., Cordella, F., and Zollo, L. (2025). Design of a testbed for mechanical and thermal stimulation in somatosensory studies. *Sci. Rep.* 15:15607. doi: 10.1038/s41598-025-00026-1.

Steidel, K., Krause, K., Menzler, K., Strzelczyk, A., Immisch, I., Fuest, S., et al. (2021). Transcutaneous auricular vagus nerve stimulation influences gastric motility: a randomized, double-blind trial in healthy individuals. *Brain Stimul.* 14, 1126–1132. doi: 10.1016/j.brs.2021.06.006.

Strzalkowski, N. D. J., Ali, R. A., and Bent, L. R. (2017). The firing characteristics of foot sole cutaneous mechanoreceptor afferents in response to vibration stimuli. *J. Neurophysiol.* 118, 1931–1942. doi: 10.1152/jn.00647.2016.

Tan, G., Adams, J., Donovan, K., Demarest, P., Willie, J. T., Brunner, P., et al. (2024). Does vibrotactile stimulation of the auricular vagus nerve enhance working memory? A behavioral and physiological investigation. *Brain Stimul. Basic Transl. Clin. Res. Neuromodulation* 17, 460–468. doi: 10.1016/j.brs.2024.04.002

Tremblay, K., Kraus, N., McGee, T., Ponton, C., and Otis, B. (2001). Central auditory plasticity: changes in the N1-P2 complex after speech-sound training. *Ear Hear.* 22, 79–90. doi: 10.1097/00003446-200104000-00001

tVNS Technologies GmbH (2025). *Is tVNS® E a Certified Medical Device? tVNS Technologies GmbH*. Erlangen: tVNS Technologies GmbH. Available online at: https://t-vns.com/training/is-tvns-e-a-certified-medical-device/ (Accessed August 27, 2026).

Tyler, W. J., Wyckoff, S., Hearn, T., and Hool, N. (2019). The safety and efficacy of transdermal auricular vagal nerve stimulation earbud electrodes for modulating autonomic arousal, attention, sensory gating, and cortical brain plasticity in humans:732529. doi: 10.1101/732529

Verma, N., Mudge, J. D., Kasole, M., Chen, R. C., Blanz, S. L., Trevathan, J. K., et al. (2021). Auricular vagus neuromodulation-a systematic review on quality of evidence and clinical effects. *Front. Neurosci.* 15:664740. doi: 10.3389/fnins.2021.664740.

Verrillo, R. T. (1966). Vibrotactile Sensitivity and the Frequency Response of the Pacinian Corpuscle ResearchGate. doi: 10.3758/BF03342215

Ward, M. P., Tan, Z., Sclocco, R., Kuo, B., Napadow, V., Nowak, T., et al. (2020). SPARC: transcutaneous auricular vagal nerve stimulation increases antroduodenal motility in rat within a narrow range of stimulus parameters. *FASEB J.* 34, 1. (1966) doi: 10.1096/fasebj.2020.34.s1.05187

Woodbury, D. M., and Woodbury, J. W. (1990). Effects of vagal stimulation on experimentally induced seizures in rats. *Epilepsia* 31, S7–19. doi: 10.1111/j.1528-1157.1990.tb05852.x

Yu, Y., Ling, J., Yu, L., Liu, P., and Jiang, M. (2021). Closed-loop transcutaneous auricular vagal nerve stimulation: current situation and future possibilities. *Front. Human Neurosci.* 15:785620. doi: 10.3389/fnhum.2021.785620.

Yücel, M. A., Selb, J. J., Huppert, T. J., Franceschini, M. A., and Boas, D. A. (2017). Functional near infrared spectroscopy: enabling routine functional brain imaging. *Curr. Opin. Biomed. Eng.* 4, 78–86. doi: 10.1016/j.cobme.2017.09.011.

Zanos, T. P., Silverman, H. A., Levy, T., Tsaava, T., Battinelli, E., Lorraine, P. W., et al. (2018). Identification of cytokine-specific sensory neural signals by decoding murine vagus nerve activity. *Proc. Natl. Acad. Sci.* 115, E4843–E4852. doi: 10.1073/pnas.1719083115.

Zhu, Y., Xu, F., Lu, D., Rong, P., Cheng, J., Li, M., et al. (2021). Transcutaneous auricular vagal nerve stimulation improves functional dyspepsia by enhancing vagal efferent activity. *Am. J. Physiol. Gastrointest. Liver Physiol.* 320, G700–G711. doi: 10.1152/ajpgi.00426.2020.